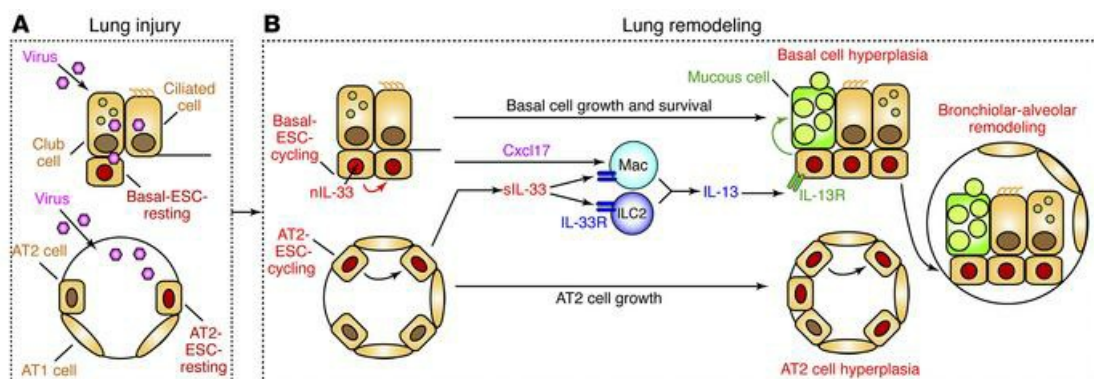# Basal epithelial stem cells cross an alarmin checkpoint for postviral lung disease

Kangyun Wu, … , Samantha A. Morris, Michael J. Holtzman

Research Article **Pulmonology**

Graphical abstract

Basal epithelial stem cells cross an alarmin checkpoint for postviral lung disease

Kangyun Wu,[1] Kenji Kamimoto,[2,3] Yong Zhang,[1] Kuangying Yang,[1,4] Shamus P. Keeler,[1] Benjamin J. Gerovac,[1] Eugene V. Agapov,[1] Stephen P. Austin,[1] Jennifer Yantis,[1] Kelly A. Gissy,[1] Derek E. Byers,[1] Jennifer Alexander-Brett,[1,5] Christy M. Hoffmann,[1] Matthew Wallace,[1] Michael E. Hughes,[1,2] Erika C. Crouch,[5] Samantha A. Morris,[2,3] and Michael J. Holtzman[1,6]

[1]Pulmonary and Critical Care Medicine, Department of Medicine, [2]Department of Genetics, [3]Department of Developmental Biology, [4]Division of Biostatistics, [5]Department of Pathology and Immunology, [6]Department of Cell Biology and Physiology, Washington University School of Medicine, Saint Louis, Missouri, USA.

Epithelial cells are charged with protection at barrier sites, but whether this normally beneficial response might sometimes become dysfunctional still needs definition. Here, we recognized a pattern of imbalance marked by basal epithelial cell growth and differentiation that replaced normal airspaces in a mouse model of progressive postviral lung disease due to the Sendai virus. Single-cell and lineage-tracing technologies identified a distinct subset of basal epithelial stem cells (basal ESCs) that extended into gas-exchange tissue to form long-term bronchiolar-alveolar remodeling regions. Moreover, this cell subset was selectively expanded by crossing a cell-growth and survival checkpoint linked to the nuclear-localized alarmin IL-33 that was independent of IL-33 receptor signaling and instead connected to autocrine chromatin accessibility. This mechanism creates an activated stem-progenitor cell lineage with potential for physiological or pathological function. Thus, conditional loss of *Il33* gene function in basal epithelial cells disrupted the homeostasis of the epithelial barrier at skin and gut sites but also markedly attenuated postviral disease in the lung based on the downregulation of remodeling and inflammation. Thus, we define a basal ESC strategy to deploy innate immune machinery that appears to overshoot the primordial goal of self-defense. Our findings reveal new targets to stratify and correct chronic and often deadly postviral disease.

Introduction

Epithelial barrier sites such as skin, gut, and lungs are charged with host protection that relies on endoderm-derived epithelial stem cells to repair any possible damage (1–3). When the injury is due to infection, this barrier is further responsible for a process that contains and helps eliminate the pathogen (4, 5). For this task, barrier epithelial cells must also communicate upstream and downstream with immune cells to coordinate the host response (6–8). If successful, a normal physiological barrier is restored in the host. However, in some cases, barrier activities might be reprogrammed toward a detrimental response that can result in disease. Indeed, a relatively stereotyped pattern of epithelial injury and acute illness that progresses to epithelial remodeling and chronic disease is well established after severe infection with respiratory viruses (9), including epidemic influenza viruses (10). In fact, morbidity and mortality due to respiratory viral infections often peak after infectious virus should be cleared and tissue repair should be completed. This delayed development of lung disease after viral infec-tion is likely a component of acute lung injury (11) but is perhaps best established for chronic remodeling and inflammatory disease as described for asthma (12) and previously proposed for long-term sequelae after influenza virus and coronavirus infections (13, 14). It is therefore critical to define whether unchecked barrier cell behavior might lead to this type of postviral lung disease (PVLD) and thereby identify targets for therapeutic correction of an extremely common and pressing health care problem.

In that regard, several populations of lung barrier epithelial cells (including airway basal and club cells and alveolar epithelial type 2 [AT2] cells as well as overlapping airway-alveolar cells) are proposed as stem cells. As a general rule, these cell populations are active in lung development and are called up again for lung regeneration as needed in later life (3, 15–23). In support of this possibility, renewed growth of basal and AT2 cells is typically found after viral infection in experimental models (mainly using influenza viruses) and clinical settings (including new coronaviruses; refs. 24–27). However, the precise molecular basis for this type of epithelial stem cell activation and its contribution to homeostatic versus pathologic outcome still needs to be defined.

Relevant to this issue, we reported the expansion of an airway progenitor epithelial cell population in a subset of patients with chronic obstructive pulmonary disease (COPD) that might also be linked to viral infection (28). This cell population expressed markers of basal cells and tracked with high-level expression of the cytokine IL-33 that activates the IL-33 receptor (designated as ST2) signaling for a type 2 immune response. In turn, this type of response can account for additional type 2 cytokine production that drives progenitor-to-mucous cell differentiation as a
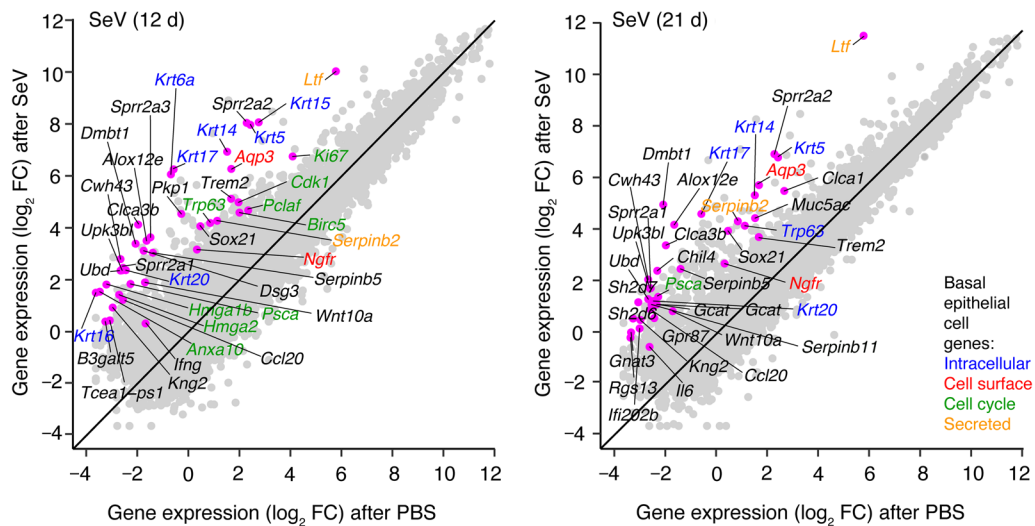
Figure 1. Induction of basal epithelial cell growth and differentiation genes after SeV infection. Gene-gene expression plots for RNA-Seq analysis of lung tissue from WT mice 12 and 21 days (d) after SeV infection versus control PBS challenge. Annotations indicate 25 genes with the greatest fold change (FC) in expression levels for SeV versus PBS (excluding immunoglobulin genes and adding informative basal epithelial cell genes, which are annotated by colors). Data represent results from a single experiment with 3 mice per condition.

key hallmark of chronic lung disease (28–30). This detrimental outcome is likely reprogrammed from the intended purpose of wound healing and host defense (31). However, it remained uncertain whether similar or distinct activation of epithelial stem cells might be (a) found after viral infection; (b) linked to tissue remodeling and/or immune cell activation as a basis for PVLD; or (c) controlled as a means to prevent this type of disease.

Here, we address this issue in studies of a mouse model of PVLD caused by the natural rodent pathogen Sendai virus (SeV). We chose this model for several reasons: (a) the pattern of acute illness progresses from proximal to distal airspaces for a bronchiolar-alveolar (centrilobular) pattern that is characteristic of natural infection (5, 32); (b) acute infectious illness is linked to progressive and long-term lung remodeling disease in a genetically susceptible but also widely engineered inbred strain (C57BL/6J) (33–35); (c) these experimental conditions allow application of highly informative single-cell, lineage-tracing, gene reporter, and conditional gene-knockout technologies; and (d) the disease components detected to date are also routinely found in other experimental models of inflammatory lung disease and in humans with respiratory disease linked to viral infection (5, 8, 10, 28–30, 36). In the present study, the combination of these advanced approaches revealed a subset of basal epithelial stem cells (basal ESCs) that are critical for homeostasis at barrier sites in skin and gut but are also reprogrammed for the excessive growth, migration, and immune activation that drive postviral disease in the lungs. Both physiological and pathological phenotypes depend on intracellular IL-33 function as a nuclear alarmin and can be segregated from secreted IL-33 actions for a feedforward type 2 immune response that promotes basal ESC differentiation into mucous cells. This pathway also combines with basal ESC–derived immune signaling for tissue macrophage recruitment, activation, and consequent inflammation. Our identification of an intersection between basal ESCs and innate immunity thus

provides an unexpected addition to the conventional paradigm for the actions of the epithelial barrier. The latest circuitry for basal ESC function also defines unexpected components that can be applied to the unmet need for a precise, disease-modifying strategy relevant to the critical problem of PVLD.

Results

Viral infection reprograms basal ESCs for continued expansion. As introduced above, we engaged a mouse model in which the peak of remodeling disease occurs 49 days after SeV infection and is well characterized at that time point using microarray-based gene expression profiling (28). Here, we took advantage of an updated RNA-Seq approach for unbiased whole-genome lung expression on day 12 after SeV infection, which might represent an earlier switch point from acute infectious illness to chronic remodeling disease, and on day 21, when the full features of the remodeling disease become detectable. The new analysis revealed prominent induction of basal-epithelial cell markers 12 days after infection, including a heretofore unrecognized increase in *Aqp3* mRNA along with conventional basal cell markers typified by *Krt5*, *Trp63*, and *Ngfr* mRNA (Figure 1 and Supplemental Figure 1; supplemental material available online with this article; https://doi.org/10.1172/JCI149336DS1). Moreover, increases in basal cell marker levels at day 12 continued to progress to maximal levels 21–49 days after infection, based on RNA-Seq and the corresponding quantitative PCR (qPCR) assay, and were correlated with subsequent mucinous differentiation marked by *Muc5ac* gene expression (Figure 2, A and B). This pattern of gene expression developed in concert with bronchiolar-alveolar sites of mucinous differentiation based on periodic acid–Schiff–hematoxylin (PAS-hematoxylin) staining 49 days after infection (Figure 2C), consistent with mucous cell formation as reported previously (5). In concert with gene expression data, these remodeling sites also contained Aqp3+Krt5+ basal cells (Figure 3A). In bronchiolar-alveolar locations, these
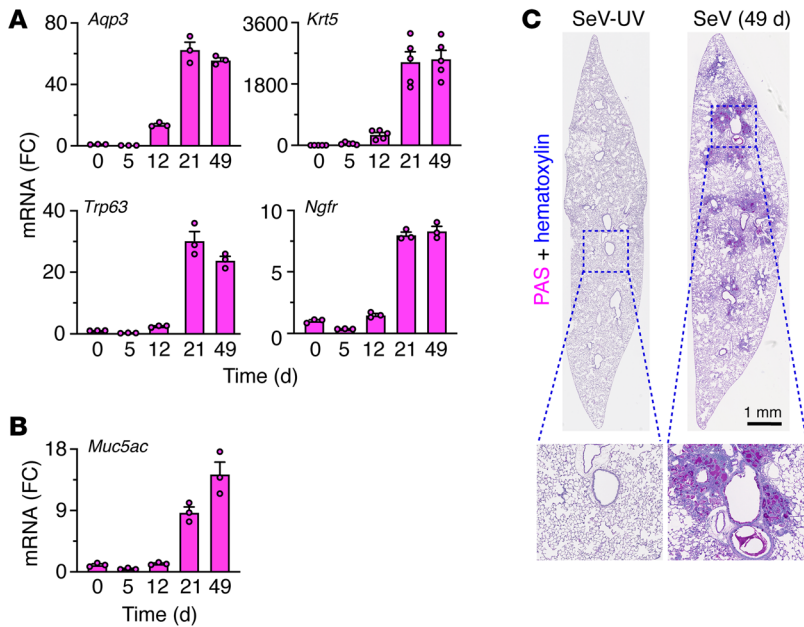
Figure 2. Basal epithelial cell expansion and mucinous differentiation after SeV infection. (**A**) Lung levels of mRNA markers for basal epithelial cells 0–49 days after SeV infection in WT mice. (**B**) Corresponding mRNA marker for mucous cells under the conditions in **A**. (**C**) PAS and hematoxylin staining of lung sections 49 days after SeV or UV-inactivated SeV (SeV-UV). Data represent results from a single experiment with 3–5 mice per condition, and experiments were replicated twice.

since this flow cytometry gate (EpCAM$^+$Aqp3$^-$) contained *Sftpc* mRNA as a validated AT2 cell marker and *Il33* mRNA as a possible marker for this population in mice (Supplemental Figure 2B).

Consistent with the preceding results for cell proliferation, EpCAM$^+$Aqp3$^+$ cells generated lung spheroids that maintained an Aqp3$^+$ basal cell phenotype in 3D organoid cultures (Figure 4G) and differentiated into Muc5ac$^+$ mucous cells in response to IL-13 under these conditions (Supplemental Figure 2, C–E). Moreover, EpCAM$^+$Aqp3$^+$ cells formed lung spheroids at higher efficiency compared with EpCAM$^+$Aqp3$^-$ cells (Figure 4H). Additional flow cytometry showed that Aqp3$^+$ cells represented a proliferative subset of Itga6$^+$ cells (Figure 4I and Supplemental Figure 2, F and G), consistent with evidence of Itga6$^+$ basal progenitor cells in mouse lung (19) and comparable cells in humans (28). Indeed, flow cytometry also showed corresponding increases in Aqp3$^+$ cells (Figure 4J), in step with cell numbers found in the lungs in situ (Figure 4K), again as a subset of Itga6$^+$ cells (Supplemental Figure 2H). Together, the results identified an Aqp3$^+$ basal ESC subset that was activated for growth in concert with AT2 cell hyperplasia as key long-term remodeling components in PVLD.

Single-cell analysis defines ESC subsets for postviral growth and differentiation. To better define virus-sensitive epithelial cell populations, we next annotated gene expression in relation to lung epithelial cell expansion using single-cell RNA-Seq (scRNA-Seq). Gene expression patterns of lung epithelial cells (CD45$^-$CD31$^-$EpCAM$^+$) across 3 sample conditions (PBS control challenge and 12 or 21 days after SeV infection) revealed 13 clusters of epithelial cells based on nearest-neighbor, heatmap, and dot plot analyses, with basal cells identified as 3 distinct cell clusters (designated clusters 1–3; Figure 5A and Supplemental Figure 3, A and B). Gene expression for each sample condition mapped onto cell-type clusters and specific cell counts for each cell population showed that basal cell cluster 3 appeared transiently on day 12, whereas basal cell clusters 1 and 2 were more prominent later, 21 days after SeV infection (Figure 5, A and B). Cell-cycle gene expression mapped onto cell-type clusters also showed a transient appearance of basal cell cluster 3 twelve days after SeV infection that coincided with the appearance of AT2 cell cluster 9 (Figure 5C). To relate basal cell proliferation and survival to ontogeny, we also used scRNA-Seq data to infer cell trajectory. For this approach, we applied partition-based graph abstraction (PAGA) (37) for a pseudotemporal ordering algorithm followed by RNA velocity analysis of single cells, based on spliced versus unspliced mRNA abundance (38). The combined analysis revealed a parental cluster 1 found at baseline that could give rise to cluster 3 and in turn clusters 1 and 2 to fully account for basal cell expansion (Figure 5D), consistent with the time course for the appearance of basal cell clusters (Figure 5, B and E) and basal cells (Figure 3G).

To further delineate a possible basal cell program for PVLD, we mapped basal cell expansion and differentiation using cell lineage tracing guided by *Krt5* as a marker of basal cell clusters (Sup-

sites excluded Sftpc$^+$ AT2 cells but still maintained podoplanin$^+$ (Pdpn$^+$) cells (Figure 3, A and B). This combination was reflected by Aqp3$^+$Pdpn$^+$ costaining in cells with basal cell morphology adjacent to Aqp3$^-$Pdpn$^+$ cells with AT1 cell morphology (Figure 3C). Together, the results indicated that basal cell expansion starts in bronchiolar sites and extends further distally to alveolar sites, as suggested for the response to influenza A virus (IAV) infection (25, 26). In parallel with this process, we also found increases in Sftpc$^+$ AT2 cells in alveolar regions (Figure 3D). Bronchiolar-alveolar remodeling was detectable on day 12 (Figure 3E) and alveolar remodeling as soon as 5 days after infection (Figure 3F), both of which were reflected by the quantitation of cell markers (Figure 3G) and are suggestive of distinct remodeling mechanisms for airway and alveolar compartments.

Relevant to this observation, analysis of lung RNA-Seq data also showed marked increases in genes connected to cell-cycle activation and progression, particularly 12 days but also 21 days after SeV infection (Figure 1). Consistent with these findings, we observed increases in lung levels of *Ki67* mRNA (Figure 4A) and Ki-67$^+$ immunostaining that also peaked at 12–14 days but continued out to 49 days after infection (Figure 4, B and C, and Supplemental Figure 2A). Tissue costaining revealed further localization of Ki-67 expression primarily to basal and AT2 cells (Figure 4, D and E), in agreement with the above-noted increases in these 2 cell populations (Figure 3G), and confirming the delay from cell-cycle activation to the change in cell numbers. Flow cytometric analysis of lung epithelial cells (CD45$^-$CD31$^-$EpCAM$^+$) demonstrated that cell proliferation marked by Ki-67 tracked primarily to a subset of Aqp3$^+$ basal cells (Figure 4F). We observed smaller fold increases in Aqp3$^-$ cells, consistent with a lower-fold expansion of AT2 cells,
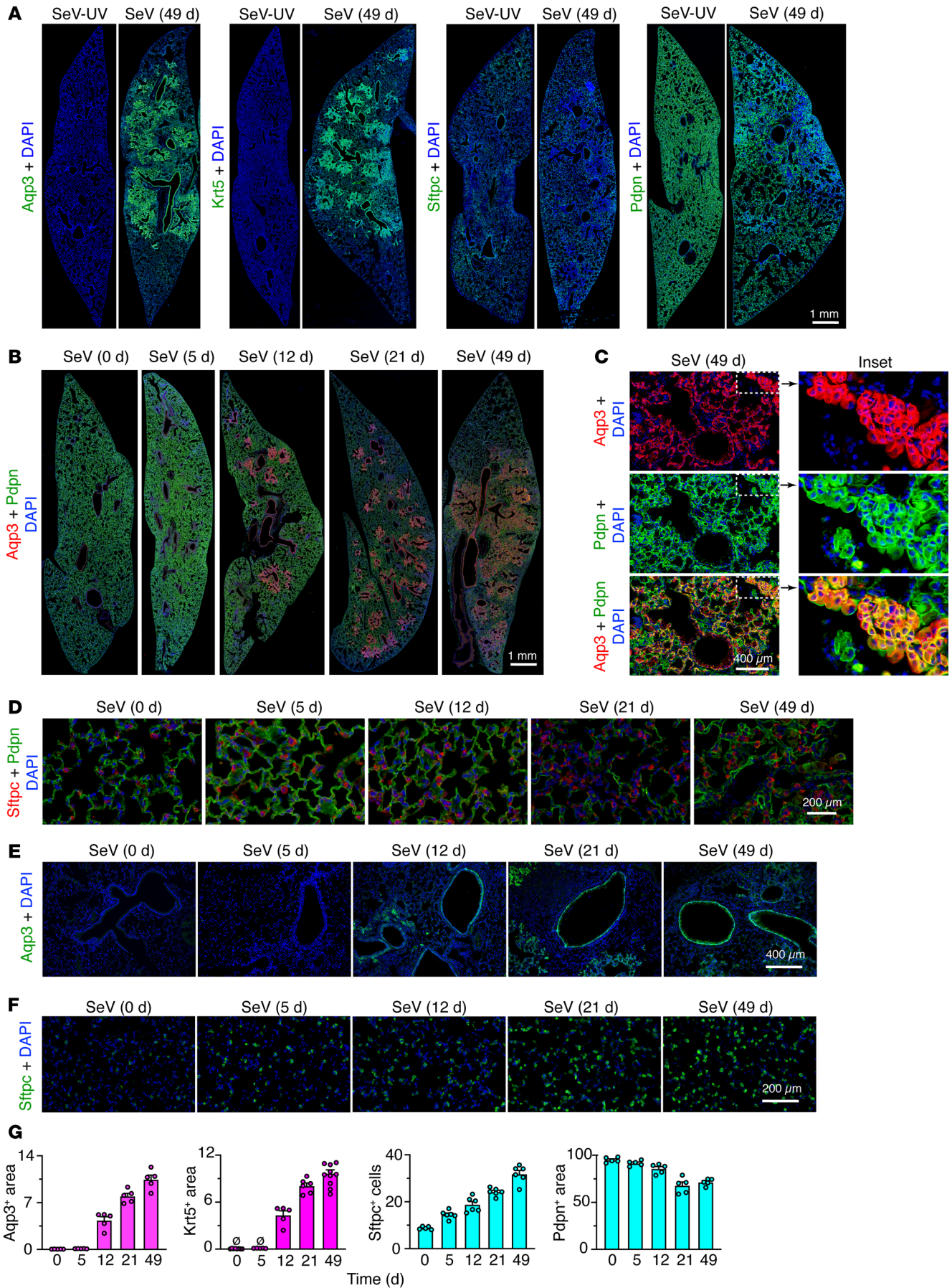
Figure 3. Progressive long-term lung remodeling after SeV infection.
(**A**) Immunostaining for Aqp3, Krt5, Sftpc, and Pdpn with DAPI counter-staining in lung sections 49 days after SeV or SeV-UV infection. Scale bar: 1 mm. (**B**) Immunostaining for Aqp3 and Pdpn in lung sections 0–49 days after SeV infection. Scale bar: 1 mm. (**C**) Immunostaining of bronchiolar-alveolar remodeling sections under the conditions in **B**. Scale bar: 400 μm. Original magnification, ×3.5 (inset). (**D**) Immunostaining for Sftpc and Pdpn in lung alveolar sections 0–49 days after SeV. Scale bar: 200 μm. (**E**) Immunostaining for Aqp3 in lung bronchiolar-alveolar sections 49 days after SeV infection. Scale bar: 400 μm. (**F**) Immunostaining for Sftpc 0–49 days after SeV infection. Scale bar: 200 μm. (**G**) Quantitation of immunostaining for Aqp3, Krt5, Sftpc, and Pdpn in lung sections 0–49 days after SeV infection. Data represent results from a single experiment with 5 mice per condition and were replicated twice.

plemental Figure 3B and Figure 5E). To validate this approach, we first showed that Aqp3+ basal cells could be efficiently (89%) marked by *Krt5* gene expression, since FACS-purified Aqp3+ cells were also Krt5+ when isolated from WT mice 21 days after SeV infection (Supplemental Figure 4, A and B). We therefore tracked the fate of *Krt5-Gfp*–labeled cells in post-SeV disease using lineage tracing with *Krt5-Cre-Ert2 ROSA26^{mTmG}* reporter mice that were marked with transient tamoxifen treatment 3 weeks before infection (Supplemental Figure 4C). We found marked Krt5-GFP+ trace into airway cells, e.g., Krt5+ and Aqp3+ basal cells, Muc5ac+ mucous cells, β-tubulin IV+ ciliated cells, and Scgb1a1+ club cells, but not into Sftpc+ AT2 cells 49 days after SeV infection (Supplemental Figure 4D). We detected no GFP signal after tamoxifen induction without infection or with SeV infection without tamoxifen, providing for specificity of the tracing signal (Supplemental Figure 4D). Colocalization of GFP with Aqp3 and Muc5ac immunostaining was confirmed with confocal microscopy (Supplemental Figure 4E) and quantified by image analysis (Supplemental Figure 4F). Lineage trace into Krt5+ basal cells was similar to the response to IAV infection (25, 26), however, a Krt5 trace into alveolar cells (as high as 72% of AT2 cells; ref. 25) after IAV was not found after SeV infection, consistent with the preservation of proximal-distal ontogeny found in lung development. Our detection of rare basal cells at baseline (Figure 5B) and of a parental cluster 1 (Figure 5D) was consistent with the consequent lineage tracing of *Krt5*-expressing cells with disease and the proposal for a stem cell population poised for repair even in the adult lung.

*ESC subset growth depends on an unexpected IL-33 checkpoint.* To address the role of basal cell expansion in PVLD, we considered that basal ESCs in humans are a source of IL-33 and, in turn, that IL-33 is required for the type 2 inflammation and mucinous differentiation that is characteristic of chronic lung disease (28). However, previous work indicated that AT2 cells, and not basal cells, might be the predominant epithelial source of IL-33 expression after the development of PVLD in mice, based on in situ hybridization and immunostaining (28, 35). Here, we reassessed this question more comprehensively using mice carrying an *Il33-cherry* reporter cassette inserted into the endogenous *Il33* gene (8), recognizing that heterozygous *Il33+/–* mice still manifest all aspects of PVLD, including basal cell hyperplasia detected by flow cytometry for EpCAM+Aqp3+ cells (Supplemental Figure 5, A and B) and tissue immunostaining for Aqp3 in lung tissue (Supplemental Figure 5C) 21 days after SeV infection. In turn, these

mice also progressed to lung remodeling disease, as revealed by qPCR assays for basal cell markers (*Aqp3*, *Krt5*, and *Trp63*), a type 2 immune response (*Il33*, *Il13*, *Arg1*, and *Trem2*), and mucinous differentiation (*Muc5ac*) (Supplemental Figure 5, D–G) together with increased mucous cell numbers, as detected by Muc5ac+ immunostaining (Supplemental Figure 5H) 49 days after SeV infection. Relevant to the cell source for IL-33 expression, lung immunostaining showed that the IL-33–cherry reporter localized to Sftpc+ AT2 cells but not to Aqp3+ or Krt5+ basal cells or Scgb1a1+ club cells in *Il33+/–* mice 21 days after SeV infection (Supplemental Figure 5I). Similarly, *Il33+/–* mice crossed with Sftpc-GFP reporter mice showed localization of IL-33 signal in Sftpc+GFP+ AT2 cells but not in Aqp3+ basal cells at baseline and with PVLD, as determined by flow cytometry (Supplemental Figure 5J). These findings were consistent with AT2 cells being a primary source for secreted IL-33 and, in turn, for the stimulation of ST2-bearing immune cells responsible for IL-13 production and the development of type 2 inflammatory disease. Moreover, the time course for these downstream events fit with the detection of *Il33* and *Il13* mRNA expression in lung tissue and IL-33 and IL-13 protein production in lung tissue and bronchoalveolar lavage fluid after SeV infection (Supplemental Figure 5, K and L).

This conventional analysis confirmed that IL-33 expression was localized in AT2 cells at baseline and during PVLD but did not yet assess earlier events during the peak of cell proliferation or provide a more global and unbiased assessment of all lung epithelial cell populations. We therefore used single-cell analysis with *t*-distributed stochastic neighbor embedding (*t*-SNE) feature plots for a more comprehensive profile of IL-33 expression. With this approach, we again found that *Il33* gene expression was predominantly localized to AT2 cells (clusters 5–9) at baseline and during PVLD (Figure 6, A and B). However, the sensitivity of this approach also revealed *Il33* expression in the subset of cell-cycling basal cells (cluster 3) that appeared in concert with cycling AT2 cells (cluster 9) twelve days after SeV infection (Figure 6, A and B). To further validate *Il33* gene expression in basal epithelial cells, we also tracked expression using IL-33–cherry reporter mice. This approach identified an IL-33–cherry+ subset of Aqp3+ basal epithelial cells based on flow cytometric analysis (Figure 6C) and immunostaining of FACS-purified cells (Figure 6D) from *Il33+/–* but not WT control mice. Further, we found a comparable IL-33+ subset of Krt5+ cells in lung tissue at bronchiolar-alveolar remodeling sites following immunostaining for the IL-33–cherry reporter (Figure 6E) and for IL-33 itself (Figure 6F). In each case, IL-33 was localized to nuclei in basal cells and was primarily detected 12 days after SeV infection, corresponding to the cell proliferation peak observed with conventional (Figure 4, A–E) and single-cell (Figure 6, A–E) approaches. The restriction of IL-33 nuclear signal to Aqp3+ basal cells, which was maximal 12 days after infection, wsd consistent with localization of this signal to the *Il33*+ cycling basal cell cluster 3 on scRNA-Seq. This finding also raised the possibility that IL-33 might be linked to the cell cycle in addition to its conventional role in immune signaling.

To investigate this question, we recognized that the assignment of IL-33 production primarily to AT2 cells in mice is distinct from humans, where IL-33 expression is not detected in AT2 cells (28). However, this difference also provided an opportunity to seg-
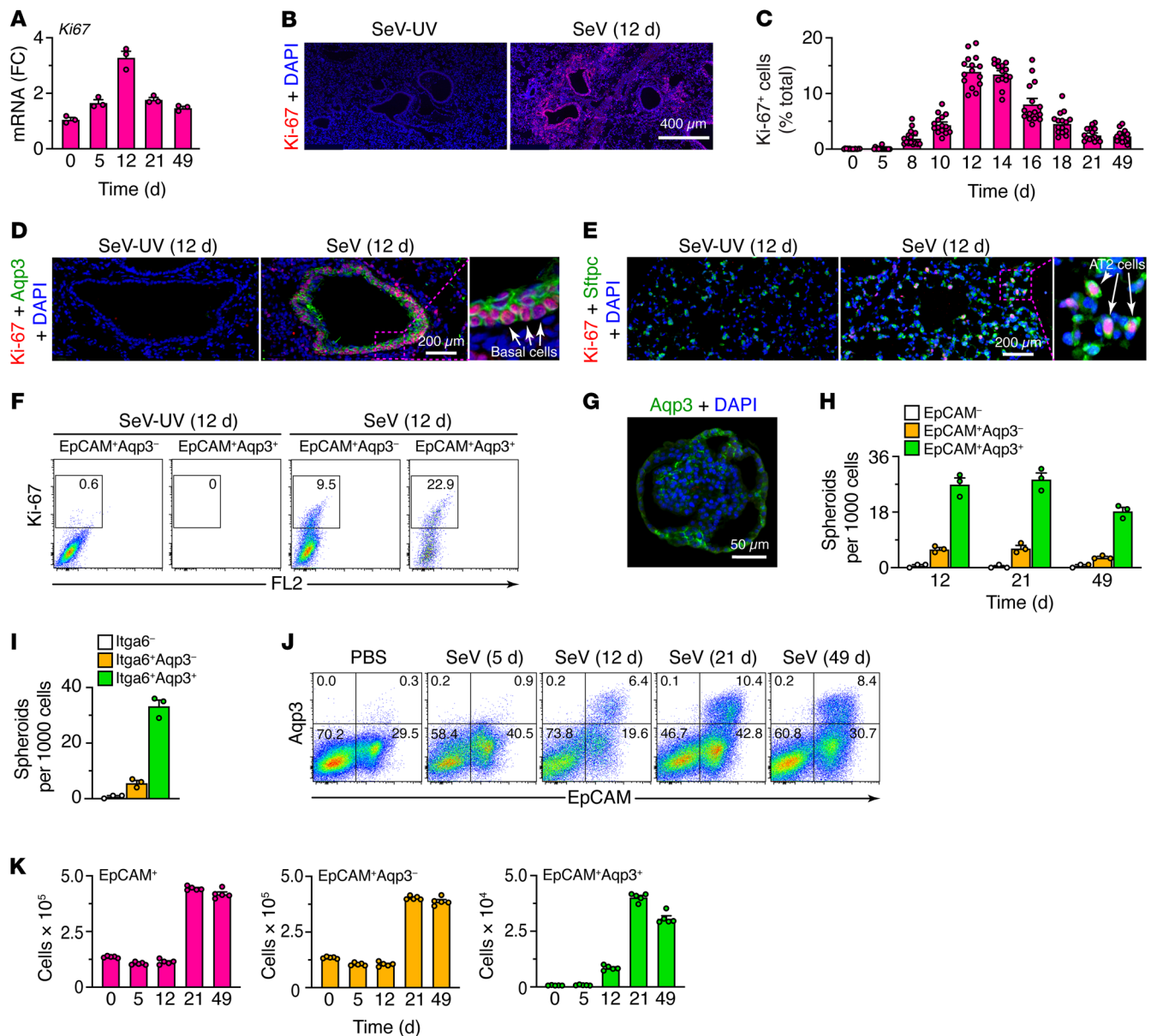
Figure 4. Basal ESC growth after SeV infection. (**A**) Levels of *Ki67* mRNA in lung tissue from WT mice 0–49 days after SeV infection. (**B**) Immunostaining for Ki-67 in lung sections 12 days after SeV infection. Scale bar: 400 μm. (**C**) Quantitation of Ki67+ cells in lung sections 0–49 days after SeV infection. (**D**) Immunostaining for Ki-67 and Aqp3 in bronchiolar-alveolar sections 12 days after SeV or SeV-UV infection. Scale bar: 200 μm. Original magnification, x3.0 (inset). (**E**) Immunostaining for Ki-67 and Sftpc in alveolar sections 12 days after SeV or SeV-UV infection. Scale bar: 200 μm. Original magnification, x3.2 (inset). (**F**) Flow cytograms for Ki-67 in lung epithelial (CD31⁻CD45⁻EpCAM⁺) cells (Aqp3⁻ and Aqp3⁺ subsets) in WT mice 12 days after SeV or SeV-UV infection. FL2, BluFL2, empty channel. (**G**) Immunostaining for Aqp3 in a lung spheroid from EpCAM⁺Aqp3⁺ cells obtained 21 days after SeV infection and placed into 3D organoid culture. Scale bar: 50 μm. (**H**) Number of lung spheroids from the indicated cell populations, obtained 12–49 days after SeV infection. (**I**) Number of lung spheroids from the indicated cell populations, obtained 21 days after SeV infection. (**J**) Flow cytograms of lung epithelial cells (CD31⁻CD45⁻ restricted and analyzed for EpCAM and Aqp3) after SeV infection or PBS treatment. Values indicate the percentage of cells within each gate. (**K**) Numbers of the indicated cell populations using the conditions in **J**. Data represent results from a single experiment with 3–5 mice per condition, and experiments were replicated twice.

regate potential differences in IL-33 function on the basis of cell type — in this case, basal cells versus AT2 cells. We therefore next assessed *Il33* gene function across lung epithelial cell populations using scRNA-Seq in homozygous *Il33⁻/⁻* mice compared with WT controls for each sample condition (PBS and 12 or 21 days after SeV infection). This analysis matrix showed a marked attenuation of basal cell expansion in *Il33⁻/⁻* mice compared with WT mice

based on a cluster analysis of combined sample conditions (Figure 7A), number of cells per cluster in each sample condition (Figure 7B), and Krt5⁺ cell counts per cluster in each condition (Figure 7C) and across all sample conditions (Figure 7D). The effect of IL-33 deficiency spared cycling basal cells in cluster 3 (and cycling AT2 cells in cluster 9) and was instead confined to basal lineage cells in clusters 1 and 2. These findings suggested an IL-33 require-
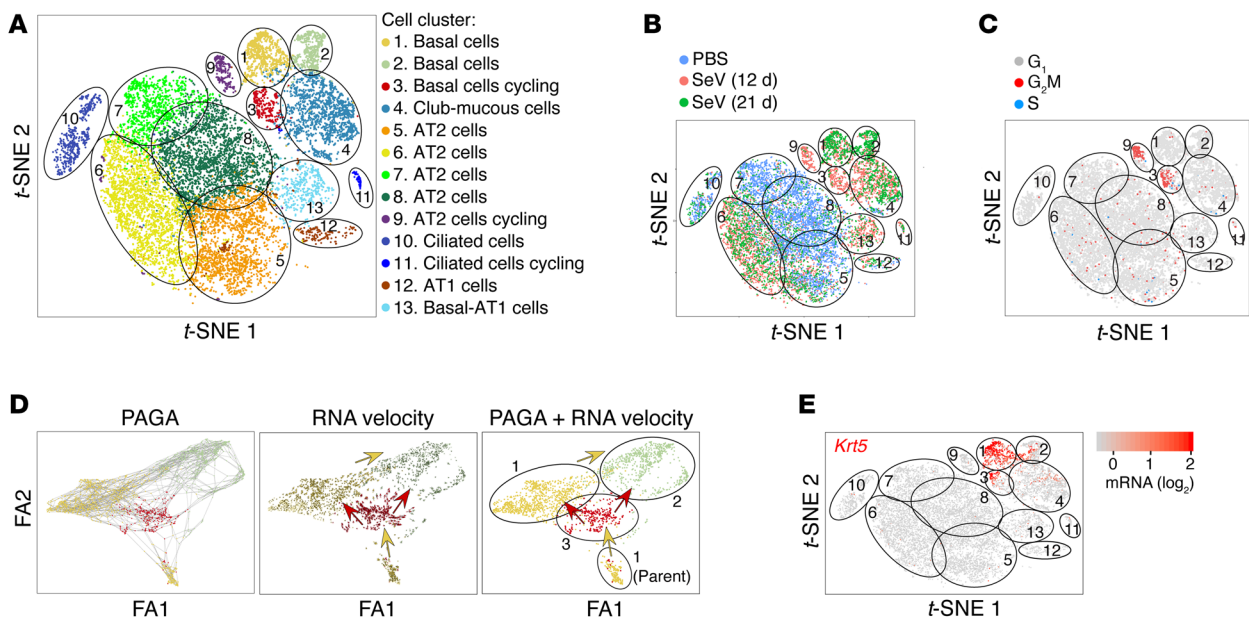
Figure 5. scRNA-Seq analysis of lung epithelial cells for growth and differentiation after SeV infection. (**A**) *t*-SNE plot for gene expression for single lung epithelial (CD45⁻CD31⁻EPCAM⁺) cells from lungs of WT mice for combined sample conditions (12 and 21 days after SeV infection or PBS treatment). Cells are colored according to the shared nearest-neighbor clusters, with cell types identified by marker gene expression. (**B**) *t*-SNE plots for gene expression for each sample condition. (**C**) *t*-SNE plots for cell-cycle (G₁, G₂M, and S phases) gene expression for combined sample conditions. (**D**) Cell trajectory analysis using combined PAGA and RNA velocity for basal cell clusters 1–3 for combined sample conditions with resolution of a parental cluster 1 subset. FA1, ForceAtlas1; FA2, ForceAtlas2. (**E**) *t*-SNE plots for *Krt5* gene expression for combined sample conditions in WT mice. Data represent results from a single experiment with 3 mice per condition.

ment for late cell-cycle progression and subsequent cell survival in downstream basal lineage cells. In support of this possibility, we found decreased expression of cell-cycle genes (e.g., *Cdk1* and *Pclaf1*) and increased expression of apoptosis genes (e.g., *Dapl1* and *Psca*) in basal cells in *Il33*⁻/⁻ mice in cycling clusters relative to WT mice (Supplemental Figure 6A). Further, this pattern of gene regulation was not found in other epithelial cell clusters, including cycling AT2 cells, where cell-cycle activation, but not cell-survival, genes were inducible and dependent on IL-33 function (Supplemental Figure 6, B and C).

Given the capacity for respiratory viral infection to regulate gene expression at the posttranscriptional level (39), we validated our findings for the corresponding control of cell growth and survival at the protein level. Here, we found that effects at the mRNA level were accurately reflected by corresponding decreases in active (phosphorylated nuclear) Cdk1 and Ki-67 (marking cell-cycle activation and cell proliferation) and increases in activated caspase-3 (marking apoptosis) in lung tissue from *Il33*⁻/⁻ mice compared with lung tissue from WT mice (Figure 8, A and B). In contrast, the *Il33* requirement for basal ESC growth found in *Il33*⁻/⁻ mice was not detected in mice deficient for the IL-33 receptor gene (*Il1rl1*⁻/⁻; Figure 8, A and B). Taken together, the findings suggested an unexpected role for intracellular versus extracellular signaling function for IL-33 in the control of the basal cell cycle after viral infection.

To further determine *Il33* gene function, we also performed a single-cell assay for transposase-accessible chromatin (ATAC) using sequencing (scATAC-Seq) and thereby defined chromatin accessibility and gene promoter activation in relation to epithelial cell clusters in WT versus *Il33*⁻/⁻ mice. We performed this analysis

12 days after SeV infection to capture the peak of *Il33* gene activation and proliferation in basal ESCs. Under these conditions, the analysis allowed for cell cluster assignments for scATAC-Seq (Supplemental Figure 7A) that correlated with scRNA-Seq based on cluster-specific markers (Supplemental Figure 7B). Further analysis using the Integrative Genomics Viewer (IGV) showed *Krt5* (and neighboring *Krt6a*) gene promoter activation (adjacent to the transcription start site) in cycling basal cells (cluster 20) from WT mice (Supplemental Figure 7C). Moreover, this signal was downregulated in the corresponding basal cell cluster from *Il33*⁻/⁻ mice and was not found in AT2 cell clusters such as cluster 19 (Supplemental Figure 7C). In contrast, *Il33* gene promoter activation was detectable in both basal cell and AT2 cell populations in WT mice but was downregulated only in basal cells (cluster 20) in *Il33*⁻/⁻ mice (Supplemental Figure 7C). This finding suggested that *Il33* gene promoter activity might be sensitive to intracellular IL-33 as we observed for cell-cycle and survival gene expression in basal cells but not AT2 cells. This result is also consistent with differences observed in *Il33* gene expression patterns between basal cells and AT2 cells. In addition, analysis revealed an enhancer region in cluster 20 that was also sensitive to *Il33* deficiency (Supplemental Figure 7C) and was best matched to a STAT3 transcription factor binding site in embryonic stem cells (40). Together, scRNA-Seq and scATAC-Seq suggested that *ll33* gene expression and function are distinct for cycling basal cells and might be linked to STAT3 activation. This scheme is consistent with the EGFR/STAT3 signal transduction for cell growth and mucinous differentiation found in the SeV mouse model and human airway epithelial cells in culture (41).
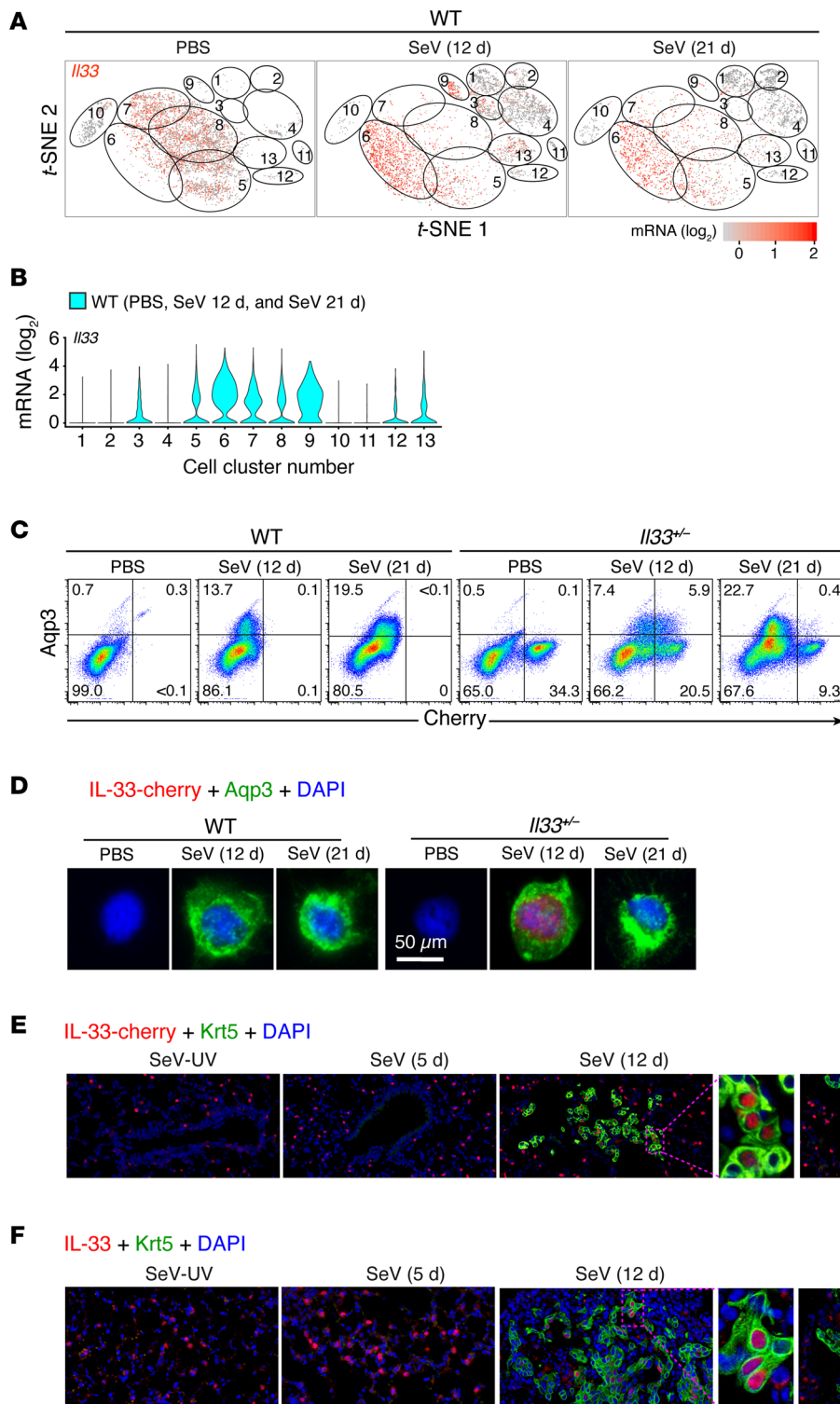
Figure 6. Single-cell analysis reveals IL-33 expression in a basal ESC subset linked to the cell cycle. (**A**) *t*-SNE plots for *Il33* gene expression in WT mice for each sample condition (PBS treatment or 12 days and 21 days after SeV infection). (**B**) Corresponding violin plots for *Il33* gene expression for the combined sample conditions in **A**. (**C**) Flow cytograms of lung epithelial cells based on Aqp3 and IL-33–cherry reporter expression in WT and heterozygous *Il33*^{+/–} mice for each sample condition. Values indicate the percentage of cells within each gate. (**D**) Immunostaining for the IL-33–cherry reporter and Aqp3 for FACS-isolated Aqp3^{+}IL-33–cherry^{+} cells under the conditions in **C**. Scale bar: 50 μm. (**E**) Immunostaining for IL-33–cherry and Krt5 in lung sections from *Il33*^{+/–} mice 5–49 days after SeV or SeV-UV infection. Scale bar: 400 μm. Original magnification, ×4.4 (inset). (**F**) Immunostaining for IL-33 and Krt5 in lung sections from WT mice 5–49 days after SeV or SeV-UV infection. Scale bar: 400 μm. Original magnification, ×3.6 (inset). For **A** and **B**, data represent results from a single experiment with 3 mice per condition; for **C–F**, data represent results from a single experiment with 5 mice per condition, and experiments were replicated twice.

Specialized IL-33 control of basal ESC subset expansion tracks with PVLD. To further define control of basal ESC expansion in relation to disease phenotype, we compared these 2 endpoints in *Il33*^{–/–} and *Il1rl1*^{–/–} mice. As with single-cell analysis, we detected a marked attenuation of Aqp3^{+} basal cell proliferation 12 days after SeV infection in *Il33*^{–/–} mice using flow cytometry to determine Ki-67 levels (Figure 9A and Supplemental Figure 8A). We found that basal cell expansion was also attenuated 12 and 21 days after

infection, again by flow cytometry for Aqp3 (Figure 9B and Supplemental Figure 8B). We observed the same pattern for stem cell function marked with lung spheroid formation in 3D organoid culture (Figure 9C). In contrast, these endpoints were not significantly affected in *Il1rl1*^{–/–} mice (Figure 9, A–C). Consistent with these findings, basal ESC formation of spheroids was unaffected by ST2 stimulation with IL-33 in 3D organoid cell culture (Supplemental Figure 8C), and *Il1rl1* mRNA and ST2 expression was undetect-
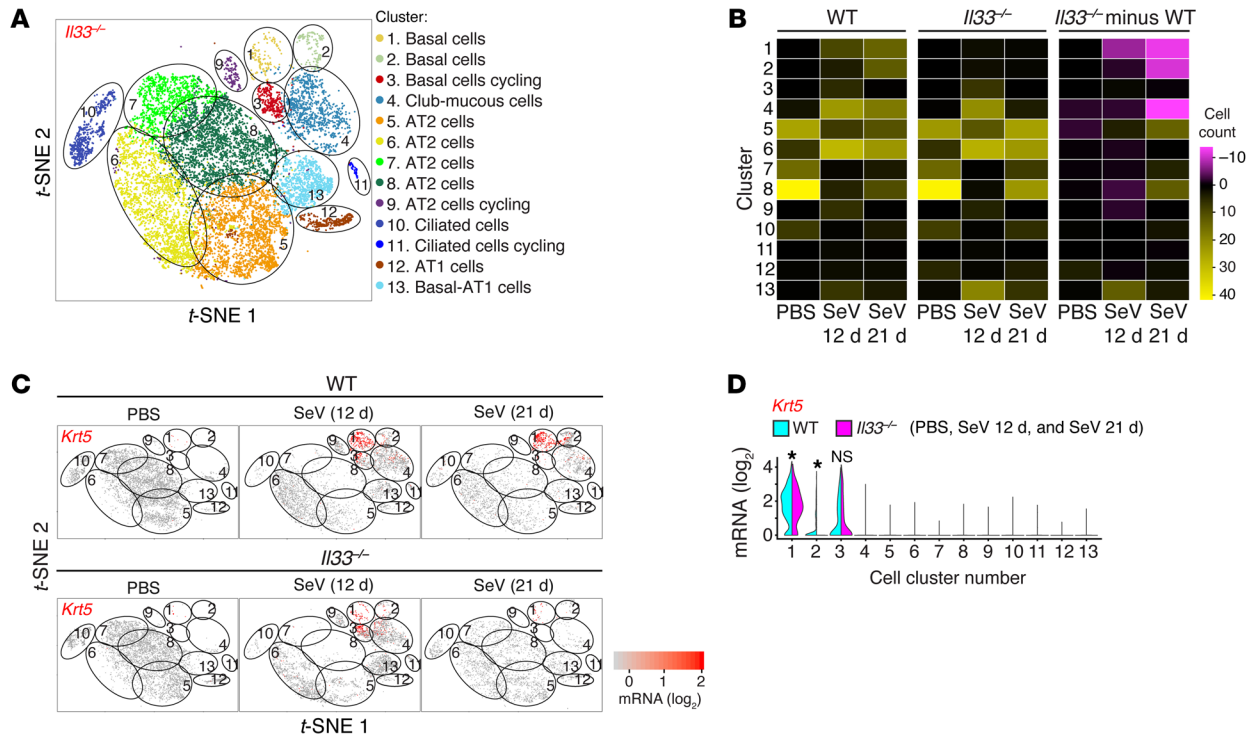
Figure 7. Comparative scRNA-Seq analysis of lung epithelial cells to link IL-33 expression to the cell cycle. (**A**) *t*-SNE plot for lung epithelial cell clusters in *Il33⁻/⁻* mice for combined sample conditions (12 and 21 days after SeV infection or PBS treatment). (**B**) Heatmap of the number of cells in each cluster for each sample condition for WT and *Il33⁻/⁻* mice and the differences between these mouse strains. (**C**) *t*-SNE plots for *Krt5* gene expression for each sample condition in WT and *Il33⁻/⁻* mice. (**D**) Violin plot for *Krt5* expression for the combined sample conditions in **C**. Data represent results from a single experiment with 3 mice per condition. *$P < 0.05$, by Mann-Whitney *U* test with Bonferroni correction.

able on epithelial cells 0–49 days after SeV infection in vivo (Supplemental Figure 8, D and E). Together, these findings provided additional in vivo and ex vivo evidence for intracellular, but not extracellular, IL-33 function as a requirement for epithelial stem cell expansion. The predominant effect on Aqp3⁺ cells further indicated a specific IL-33 control over the subset of basal ESCs.

We also observed intracellular IL-33 control over basal ESC expansion in situ. In this case, Aqp3 immunostaining of lung sections showed marked attenuation in *Il33⁻/⁻* mice compared with WT or *Il1rl1⁻/⁻* mice with preservation of IL-33–cherry⁺ AT2 cells 21 days after SeV infection (Figure 9D). Moreover, lung sections showed marked attenuation of Krt5⁺ basal cells in *Il33⁻/⁻* mice but not in *Il1rl1⁻/⁻* mice 49 days after SeV infection (Figure 9, E and F). In contrast, we found that Sftpc⁺ AT2 cell expansion in WT mice was unaffected in *Il33⁻/⁻* and *Il1rl1⁻/⁻* mice (Figure 9F and Supplemental Figure 8F). In concert with the lower basal ESC levels, *Il33⁻/⁻* mice manifested lower induction of lung mRNA markers for basal cells (Supplemental Figure 9A), knockout of *Il33* expression (Supplemental Figure 9B), and downregulation of markers for the type 2 immune response (Supplemental Figure 9C) and mucus production (Supplemental Figure 9D). Meanwhile, the levels of mRNA markers for basal cells (Supplemental Figure 9E) and *Il33*-expressing AT2 cells (Supplemental Figure 9F) were unaffected in *Il1rl1⁻/⁻* mice, despite a disruption of type 2 immune activation (Supplemental Figure 9G) and mucus production (Supplemental Figure 9H). Along with changes at the mRNA level, we noted a marked attenuation of lung histopathology in *Il33⁻/⁻* mice based on

PAS staining for mucus production and hematoxylin staining for cellularity (Supplemental Figure 9I). We confirmed these observations with a corresponding quantitative morphologic analysis (Supplemental Figure 9J). We observed similar, albeit slightly less, attenuation of histopathology based on PAS⁺ and hematoxylin⁺ staining in *Il1rl1⁻/⁻* mice (Supplemental Figure 9, I and J), indicating the relative insensitivity of this approach for specific monitoring of basal ESC expansion and its possible functional role in PVLD. Indeed, we readily detected a correction of Aqp3⁺ basal cell expansion and bronchiolar-alveolar remodeling in *Il33⁻/⁻*, but not *Il1rl1⁻/⁻*, mice by immunostaining (Supplemental Figure 9K). We also confirmed the lack of influence on Sftpc⁺ AT2 cell expansion in these mouse strains using this approach (Supplemental Figure 9, K and L). Correction of basal ESC expansion was associated with attenuation of airway hyperreactivity in *Il33⁻/⁻* compared with WT mice 49 days after infection (Supplemental Figure 9, M and N), a sign of functional benefit that was also not found in *Il1rl1⁻/⁻* mice in a previous study (28). These findings suggest a special role for basal ESC expansion in controlling barrier responsiveness.

Basal ESC function is required for homeostasis and PVLD. To fully assign barrier function and/or dysfunction to IL-33–controlled basal ESCs, we undertook a genetic strategy for selective inactivation of this cell population. Thus, we crossed *Krt5-Cre-Ert2* mice with newly generated *Il33^{fl/fl}* mice (Supplemental Figure 10, A and B) to generate *Krt5-Cre-Ert2 Il33^{fl/fl}* mice for conditional deletion of *Il33* in *Krt5*-expressing basal cells using a tamoxifen treatment scheme with a 3-week drug washout period (Supplemental Figure
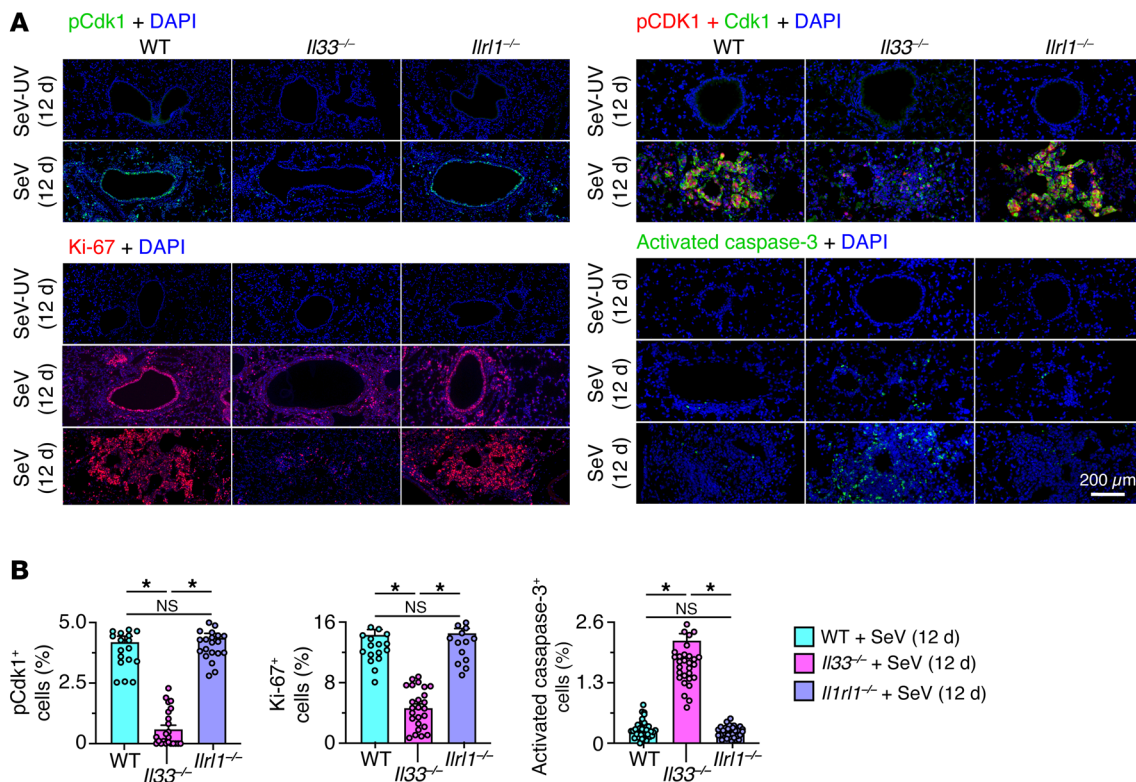
Figure 8. Protein-level validation of IL-33 linkage to cell-cycle activation and progression. (**A**) Immunostaining for phosphorylated Cdk1, as well as Cdk1, Ki-67, and activated caspase-3 with DAPI counterstaining of lung sections from mice of the indicated strains 12 days after SeV or SeV-UV infection. Scale bar: 200 μm. (**B**) Quantitation of the percentage of lung cells that stained positive for the protein markers in **A**. Data represent results from a single experiment with 5 mice per condition, and experiments were replicated twice. *$P < 0.05$, by ANOVA with Bonferroni correction.

10C). We found that tamoxifen-treated *Krt5-Cre-Ert2 Il33$^{fl/fl}$* mice had hair loss that did not occur in *Il33$^{-/-}$* mice, suggesting developmental compensation in nonconditional gene-knockout mice. Hair loss was accompanied by loss of Krt5$^+$IL-33$^+$ basal cells in the skin, but not Krt5$^+$IL-33$^-$ basal cells in the esophagus or trachea in tamoxifen-treated *Krt5-Cre-Ert2 Il33$^{fl/fl}$* mice (Supplemental Figure 10D). We also did not observe this phenotype in *Il33$^{-/-}$* mice, but it could be reproduced in *Krt5-Cre-Ert2 Rosa-DTA* mice with diphtheria toxin–driven loss of basal cells at all sites (Figure 10D). Disruption of basal cell populations in skin resulted in epithelial damage (accounting for the hair loss) and esophageal damage (resulting in ulceration) in both *Krt5-Cre-Ert2 Il33$^{fl/fl}$* and *Krt5-Cre-Ert2 Rosa-DTA* mice (Supplemental Figure 10E), consistent with estrogen-dependent control over basal cell–mediated maintenance of the epithelial barrier at this site (42). Together, these findings suggest that IL-33$^+$ basal ESCs contribute to barrier maintenance under homeostatic conditions in the skin and gut but not in the trachea.

Given the clear basal cell phenotypes of *Krt5-Cre-Ert2 Il33$^{fl/fl}$* mice at baseline, we applied the same protocol for tamoxifen treatment to delete IL-33–dependent basal cells followed by a 3-week washout period leading up to viral infection (Figure 10A). Under these conditions, neither tamoxifen-treated nor untreated *Krt5-Cre-Ert2 Il33$^{fl/fl}$* mice showed significant differences in the clinical signs or weight loss that develop after SeV infection (Figure 10B) or in lung levels of SeV-*NP* RNA (Figure 10C). However, the usual Aqp3$^+$ basal cell expansion 21 days after SeV infection

as monitored by flow cytometry was significantly attenuated in tamoxifen-treated *Krt5-Cre-Ert2 Il33$^{fl/fl}$* mice (Figure 10D). There was no significant change in the corresponding increases in Aqp3$^-$ cells (in a gate that included AT2 cells), thus confirming the treatment's specificity (Figure 10D). Similarly, basal cell proliferation (based on Ki-67 immunostaining; Figure 10E) and consequent cell numbers (based on Krt5 immunostaining; Figure 10F) were markedly downregulated, without affecting the expression of comparable markers of AT2 cells (Figure 10G) in tamoxifen-treated mice, as confirmed by quantitative morphology (Figure 10H). Tamoxifen-treated mice also showed a marked downregulation of mRNA markers of basal cells (Figure 11A), with no effect on the expression of the AT2 cell marker IL-33 (Figure 11B), still attenuated expression of markers of type 2 inflammation (Figure 11C) and mucus production (Figure 11D), and the associated lung histopathology (Figure 11, E and F). In addition, the usual Aqp3$^+$Pdpn$^+$ cell accumulation in bronchiolar-alveolar remodeling regions, but not the associated Sftpc$^+$ AT2 hyperplasia in alveolar sites, was also markedly decreased 49 days after infection (Figure 11, G and H). In line with a correction of the cellular phenotypes of disease, we also found functional improvements marked by corrections in blood oxygen desaturation (Figure 11I) and airway hyperreactivity (Figure 11J) in tamoxifen-treated, basal cell–depleted mice compared with control mice 49 days after SeV infection.

A distinct feature of *Krt5-Cre-Ert2 Il33$^{fl/fl}$* mice was the capacity for attenuation of PVLD despite a preserved induction of *Il33*
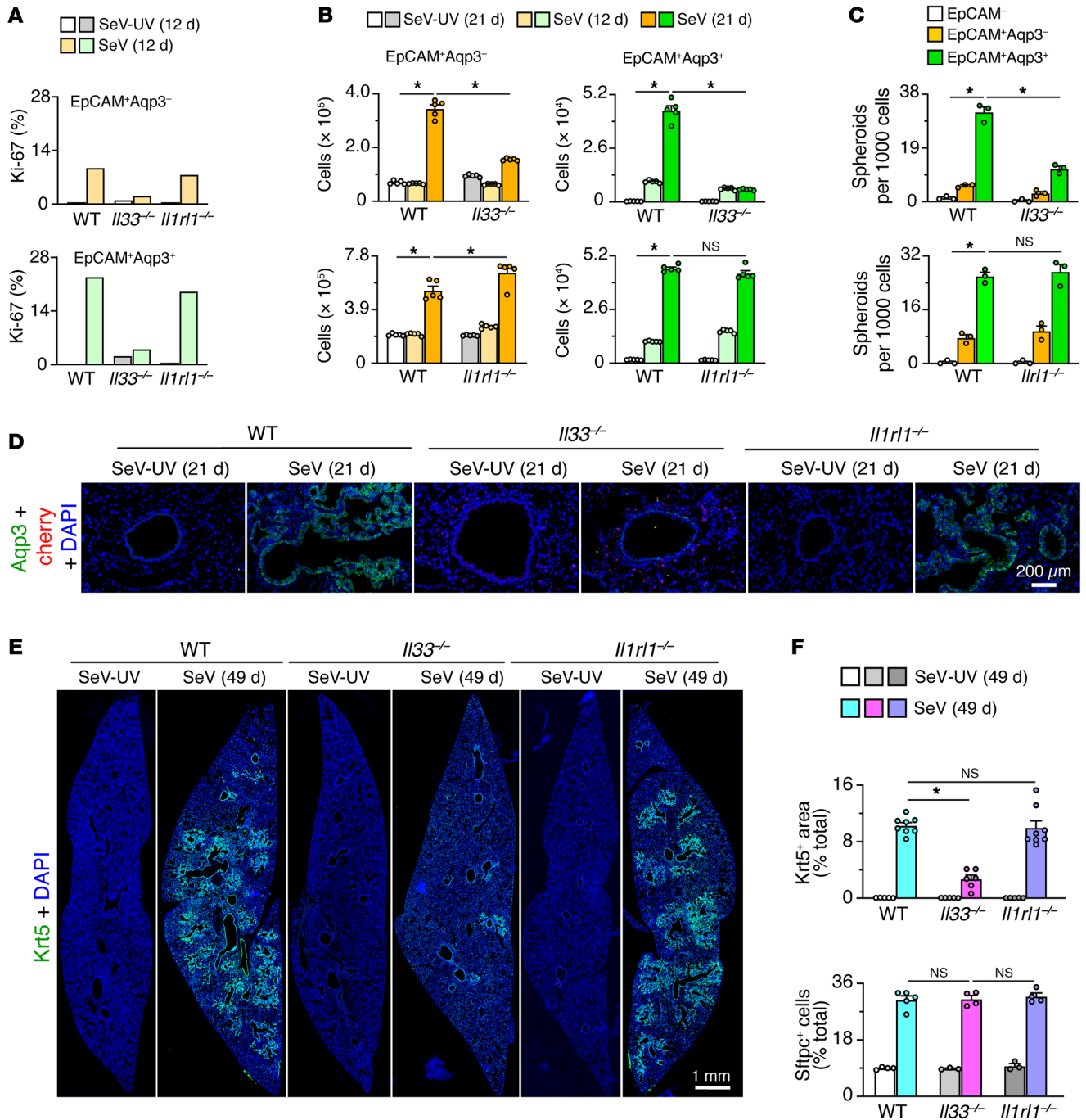
Figure 9. IL-33–dependent basal ESC expansion in PVLD. (**A**) Proliferation levels determined by flow cytometry of lung epithelial cells based on Ki-67 expression for WT versus *Il33*−/− and *Il1rl1*−/− mice 12 days after SeV versus SeV-UV infection. (**B**) Corresponding cell numbers from flow cytometry of lung epithelial cells based on Aqp3 and EpCAM expression 12 and 21 days under the conditions in **A**. (**C**) Corresponding day-21 lung spheroid formation for FACS-purified cell populations under the conditions in **A**. (**D**) Immunostaining for Aqp3 and the IL-33–cherry reporter (cherry) in lung sections under the conditions in **A**. Scale bar: 200 μm. (**E**) Immunostaining for Krt5 in lung sections 49 days after SeV or SeV-UV infection under the conditions in **A**. Scale bar: 1 mm. (**F**) Quantitation of Krt5 and Sftpc staining under the conditions in **E**. Data represent results from a single experiment with 3–8 mice per condition, and experiments were replicated twice. *P < 0.05, by ANOVA with Bonferroni correction.

expression (Figure 11B). This combination was distinct from disease blockade in *Il33*−/− mice, raising the possibility that basal cells might be activated to also influence IL-33–responsive immune cells. Indeed, macrophage accumulation marked by F4/80 immunostaining was significantly attenuated in lung sections from tamoxifen-treated versus untreated *Krt5-Cre-Ert2 Il33*fl/fl mice

(Figure 12, A and B). Moreover, the pattern of macrophage accumulation resembled the localized sites of basal cell expansion and remodeling (based on similar regional changes shown in Figure 10F, Supplemental Figure 9, I and K, and Figure 12A). As a basis for this effect, scRNA-Seq revealed that the macrophage chemokine *Cxcl17* was induced primarily in basal cells and the basal cell–
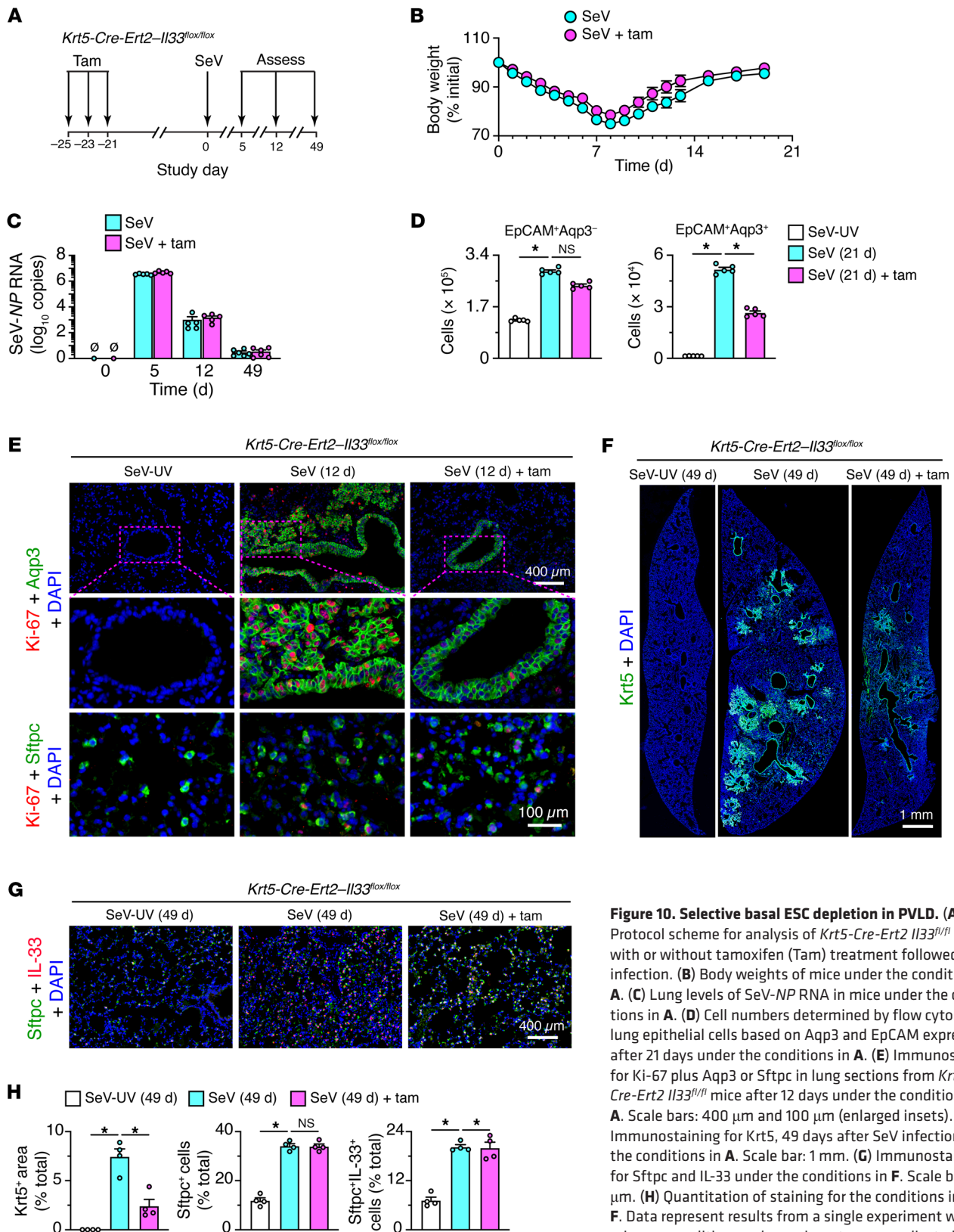
Figure 10. Selective basal ESC depletion in PVLD. (A) Protocol scheme for analysis of *Krt5-Cre-Ert2 Il33*^{fl/fl} mice with or without tamoxifen (Tam) treatment followed by SeV infection. (B) Body weights of mice under the conditions in A. (C) Lung levels of SeV-*NP* RNA in mice under the conditions in A. (D) Cell numbers determined by flow cytometry of lung epithelial cells based on Aqp3 and EpCAM expression after 21 days under the conditions in A. (E) Immunostaining for Ki-67 plus Aqp3 or Sftpc in lung sections from *Krt5-Cre-Ert2 Il33*^{fl/fl} mice after 12 days under the conditions in A. Scale bars: 400 μm and 100 μm (enlarged insets). (F) Immunostaining for Krt5, 49 days after SeV infection for the conditions in A. Scale bar: 1 mm. (G) Immunostaining for Sftpc and IL-33 under the conditions in F. Scale bar: 400 μm. (H) Quantitation of staining for the conditions in E and F. Data represent results from a single experiment with 4–5 mice per condition, and experiments were replicated twice. *$P < 0.05$, by ANOVA with Bonferroni correction.

derived lineage (Figure 12C). Thus, *Cxcl17* mRNA levels were 100-fold higher in the basal cell lineage than in the AT2 cell lineage. In addition, lung levels of *Cxcl17* were attenuated (Figure 12D) in the same pattern as for macrophage accumulation (Figure 12B). Further, mRNA induction identified with scRNA-Seq of EpCAM+ epithelial cells was linked to Cxcl17 protein expression localized to Aqp3+ bronchiolar and bronchiolar-alveolar remodeling regions in lung sections 49 days after SeV infection (Figure 12E). Together, the findings establish basal ESC capabilities of homeostatic function at epithelial barrier sites in skin and gut under baseline conditions but, alternatively, of remodeling and inflammatory disease activities at a corresponding barrier site in the lung after respiratory viral infection.

Discussion

To address the role of barrier epithelial cells in host protection versus disease, we performed comprehensive single-cell and transgenic analyses of a mouse model of lung disease that develops after a characteristic centrilobular pattern of infection with a natural respiratory pathogen. We compared the findings with barrier behavior at baseline without infection in lung, skin, or gut sites. The combined approach identified a distinct subset of basal ESCs that maintain skin and gut barriers under normal conditions and instead orchestrates remodeling and inflammatory disease in the lung after severe viral infection. In both cases, basal ESCs cross an IL-33–linked checkpoint for cell growth and survival. In the case of viral infection in the lung, a subset of basal ESCs engaged this mechanism to jump the usual bronchiolar-alveolar junction and grow into contiguous airspaces as a new site for mucinous differentiation and immune activation. The mouse model was critical to defining each of these homeostatic and pathologic components and especially to segregating intracellular versus extracellular IL-33 function in barrier epithelial cell activities as depicted in a summary scheme (Figure 13). Here, we developed 4 key points in this scheme derived from these observations and provide the relevance to barrier maintenance and postviral disease in general, given the overlap with phenotypes across a broad spectrum of lung diseases linked to respiratory viral infections (5, 10–14, 27, 28, 36, 41, 43).

The first of these 4 points relates to the understanding of epithelial cell hyperplasia as a characteristic feature of the response to respiratory viral infection. In mouse models of IAV infection, others recognized that basal epithelial cell hyperplasia could extend to alveolar sites (24) and might reflect a basal progenitor–to–alveolar daughter cell pathway for alveolar repair and functional improvement (25). Related work on the IAV model showed that basal cell expansion might depend on Notch signaling and yield suboptimal alveolar repair (26, 44), whereas another study of IAV found that Wnt-responsive alveolar epithelial progenitor cells within the AT2 cell lineage might be responsible for alveolar regeneration (45). Here, we examined the SeV model to address each of these issues and found that (a) subsets of both basal and AT2 cells were activated for long-term hyperplasia after viral infection; (b) the activated basal cell lineage was not traced into AT2 cells, perhaps consistent with studies of lung development and injury that preserve the bronchiolar-alveolar junction (23, 46); (c) basal cell hyperplasia extended with time to

bronchiolar-alveolar sites and was not associated with upregulation of Notch pathway components based on genomic analyses; (d) AT2 cells were absent from bronchiolar-alveolar remodeling sites, whereas AT2 cell hyperplasia developed at separate alveolar remodeling sites; (e) segregated basal and AT2 cell expansion sites fit with a distinct molecular control of these cell populations vis à vis growth and survival requirements for IL-33 function; and (f) selective blocking of basal ESC activation via conventional or conditional loss of *Il33* gene function improved remodeling (including mucinous differentiation), inflammation (including macrophage infiltration), and function (including hyperreactivity and hypoxia) as readouts of PVLD. Together, these findings reveal the independent nature of basal and AT2 cell hyperplasia and the consequent remodeling and repair endpoints. Whether this paradigm might differ for IAV infection still needs to be defined, but it nonetheless provides mechanistic guidance for generally descriptive single-cell data in humans with lung disease (47) as discussed further below.
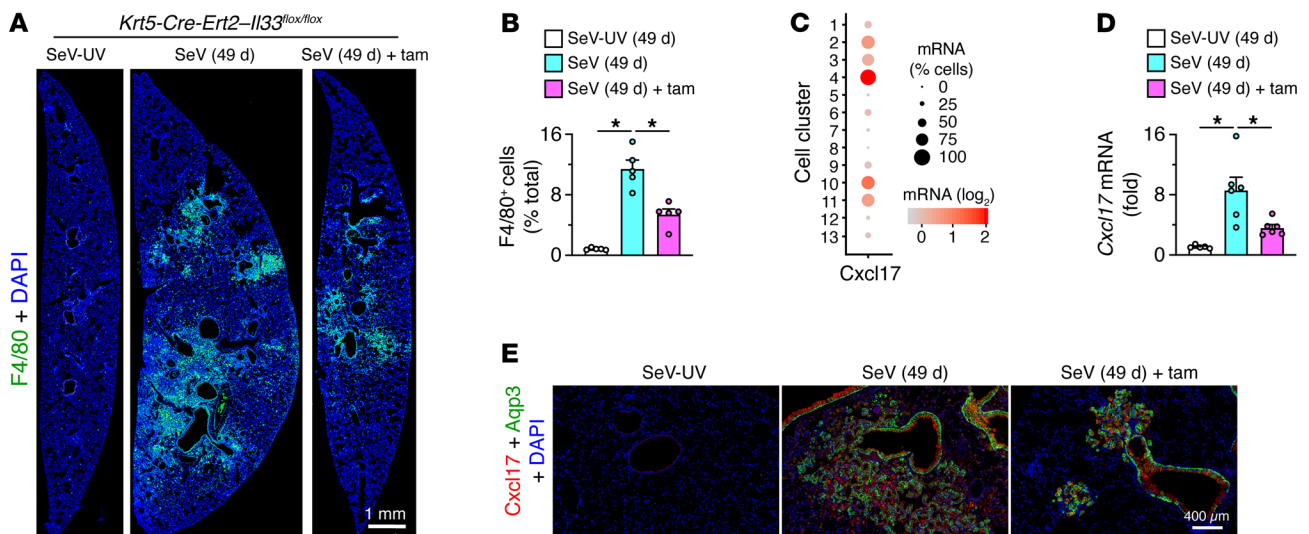
The second key point of our work also relates to the question of mechanism, as we identified a basal ESC requirement for the nuclear alarmin IL-33 in cell growth and survival in baseline conditions and after viral infection. This connection was unexpected, given the conventional view of IL-33 as an extracellular cytokine that signals to its ST2 receptor for a type 2 immune response charged for tissue repair (48–51). The alternative possibility of a nuclear signal was proposed in cell culture studies of nuclear IL-33 binding to mitotic chromatin and the regulation of gene transcription via histone modification and transcription factor binding (52–54). Another report discounted this function in endothelial cell cultures (55), but none of these previous studies focused on airway epithelial cells or viral infection, nor did they take advantage of any cell-type differences in IL-33 function. Here, we identified a role for nuclear IL-33 based on several lines of evidence: (a) *Il33* but, not *Il1rl1*, gene knockout resulted in the attenuation of basal cell activation of growth and survival genes; (b) the localization of IL-33 to basal cell nuclei corresponded in space and time to basal cell activation; (c) the effect of IL-33 on basal cells was maximal when secreted IL-33 levels were still undetectable; and (d) *Il33* gene knockout resulted in loss of the expected chromatin accessibility signal selectively in a cycling population of basal epithelial cells. Together, these findings are most compatible with the idea that IL-33 exerts nuclear control of cell-cycle activation and cell survival via autocrine signaling that is separate from extracellular ST2 activation via paracrine signaling. Additional work is needed to link IL-33 to specific interactions with nuclear proteins and epigenetic modification as a basis for immune training of basal ESCs, as found in innate immune cells. However, our data on chromatin accessibility at the *Il33* gene promoter and enhancer regions (including the potential for STAT3-binding sites) provide a roadmap for addressing the regulation of *IL33* and IL-33 target genes. Our study showing that nuclear IL-33 function is required for basal but not AT2 cell growth provides an initial molecular basis for distinct responses of these cell populations to lung injury.

The third notable point of our findings relates to the interaction of basal ESCs with immune cell partners. As discussed above, previous work highlighted the role of macrophages
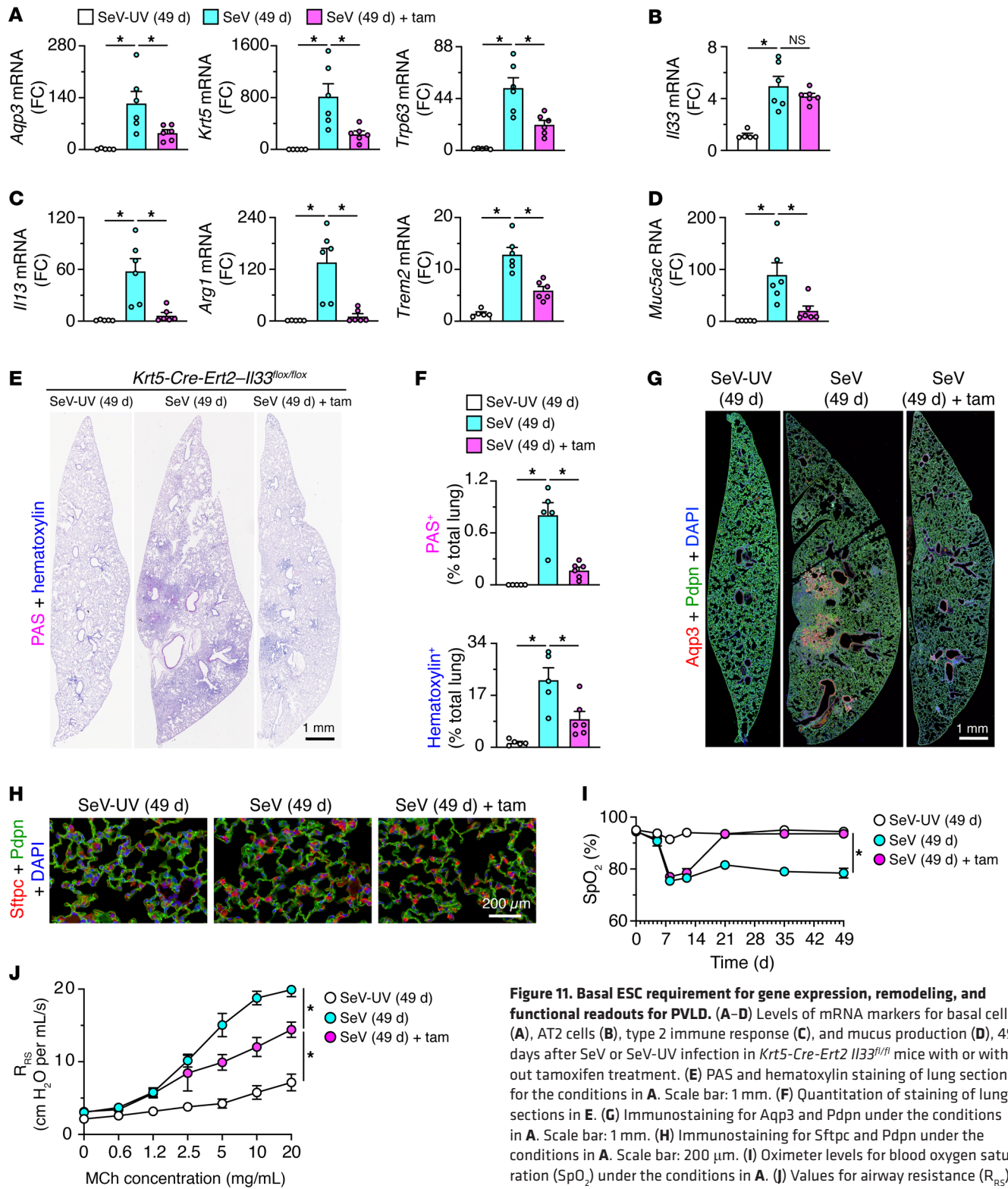
Figure 11. Basal ESC requirement for gene expression, remodeling, and functional readouts for PVLD. (**A**–**D**) Levels of mRNA markers for basal cells (**A**), AT2 cells (**B**), type 2 immune response (**C**), and mucus production (**D**), 49 days after SeV or SeV-UV infection in *Krt5-Cre-Ert2 Il33^fl/fl^* mice with or without tamoxifen treatment. (**E**) PAS and hematoxylin staining of lung sections for the conditions in **A**. Scale bar: 1 mm. (**F**) Quantitation of staining of lung sections in **E**. (**G**) Immunostaining for Aqp3 and Pdpn under the conditions in **A**. Scale bar: 1 mm. (**H**) Immunostaining for Sftpc and Pdpn under the conditions in **A**. Scale bar: 200 μm. (**I**) Oximeter levels for blood oxygen saturation (SpO$_2$) under the conditions in **A**. (**J**) Values for airway resistance (R$_{RS}$) at baseline and after inhaled MCh under the conditions in **A**. Data represent results from a single experiment with 5 mice per condition, and experiments were replicated twice. *$P < 0.05$, by ANOVA with Bonferroni correction.

Figure 12. Basal ESC immune-signaling function in PVLD. (**A**) Immunostaining for F4/80 on day 49 after SeV or SeV-UV infection of *Krt5-Cre-Ert2 Il33^{fl/fl}* mice with or without tamoxifen treatment. Scale bar: 1 mm. (**B**) Quantitation of staining for the images in **A**. (**C**) Dot plot for *Cxcl17* gene expression from scRNA-Seq analysis of lung epithelial cells for combined sample conditions (12 and 21 days after SeV infection or PBS challenge). (**D**) Lung levels of *Cxcl17* mRNA for the conditions in **A**. (**E**) Immunostaining for Cxcl17 and Aqp3 in lung sections after 49 days under the conditions in **A**. Scale bar: 400 μm. Data represent results from a single experiment with 5 mice per condition, and experiments were replicated twice. *$P < 0.05$, by ANOVA with Bonferroni correction.

(including IL-33/ST2 signaling to macrophages) in tissue repair (48–51). However, an alternative pathway toward remodeling disease was less certain. In that regard, recent studies of SeV infection serve to establish distinct roles for innate lymphoid (ILC2) and myeloid (tissue macrophage and monocyte-derived DC [moDC]) contributions to PVLD (8, 35). Our results add that IL-33+ basal cells might be key to recruiting macrophages and DCs and might do so by induction of *Cxcl17*, a chemokine gene first identified on the basis of lung mucosal expression and function in mice and humans (56, 57). Indeed, we found that Cxcl17 induction and macrophage accumulation marked bronchiolar-alveolar remodeling regions in PVLD. In addition to downstream effector signals for macrophage infiltration, recent work also identifies moDCs that are virus activated to provide an upstream immune cell niche for AT2 cells after viral infection (35). This effect would generally be attributed to an effect on cell growth and/or survival, but a signal for epithelial cell movement to distal airspaces might also be critical in the case of basal ESCs. Indeed, other chemokines (notably CCL5) can provide both survival and migration signals to airway epithelial cells and macrophages after respiratory viral infection in mouse and human models (6). Therefore, it will be of interest to further define function and track the expression of Cxcl17 and as-yet undefined niche components in PVLD in mouse models and humans.

To extend this point, the fourth implication of our study derives from the translation of experimental data to clinical conditions exemplified by lung conditions ranging from acute lung injury to chronic remodeling disease. As noted above, our paradigm for PVLD appears to hold in varying forms across a broad sample of RNA viruses (IAV, SeV, enterovirus D68 [EV-D68], respiratory syncytial virus [RSV], human rhinovirus [HRV], and severe acute respiratory syndrome–coronavirus [SARS-CoV]) studied in our laboratory and others' (5, 10, 58–60). The present data therefore link acute viral pneumonia to chronic bronchiolization, as suggested in descriptive reports of presumed viral infection (11) and documented SARS-CoV-2 infection (27, 43). Similarly, the recently reported proteomic expression of CTSL1 in COVID-19 lung tissue (61) and *TNFRSF12A* in basal cell–derived organoids (62) was also identified in our SeV model (in basal cell cluster 2), thus assigning a cell location in vivo and again underlining the stereotyped epithelial cell response to severe respiratory viral infections. The data also fit with the capacity of basal progenitor cell clones to cause inflammation, fibrosis, and mucinous differentiation when transplanted from patients with lung disease into mouse lung (63). Here, we proved this concept in vivo with the identification of a subset of basal ESCs that were modified by viral infection as a requirement for lung remodeling disease in experimental models designed to mimic the features of PVLD in humans. Studies are needed and are currently underway to determine whether similar cell and molecular events might be found after influenza virus and coronavirus infection in animal models and humans.

In summary, we anticipate that our findings will provide a new perspective on epithelial barrier function and a mechanistic basis for marking and correcting PVLD. To place the present findings in perspective, we recognize that mucociliary removal and epithelial wound responses represent some of the most ancient systems for defending against environmental injury. However, there might also be sufficient evolutionary pressure for an innate walling-off response that it can transform to drive remodeling disease under some circumstances. Thus, the present paradigm connects the primordial role of the epithelial barrier to the aberrant disease process found in susceptible hosts based on specific cell and molecular events. As an example, stress kinases such as MAPK13 might regulate both epithelial cell growth and mucinous differentiation and might therefore provide a suitable target for intervention and for defining additional factors that regulate progressive tissue
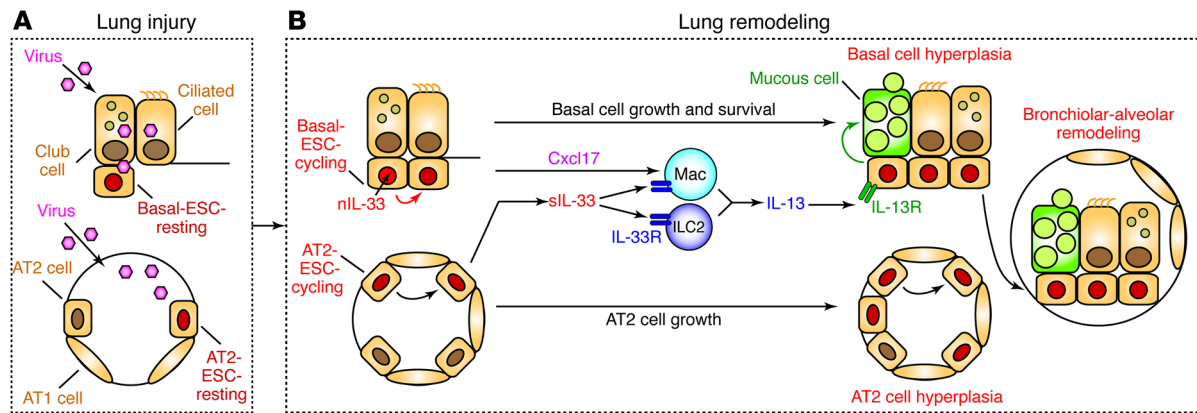
Figure 13. Scheme for the role of basal ESCs in PVLD. Key steps include (**A**) lung injury due to acute viral infection with damage to bronchiolar and alveolar epithelial cells and (**B**) lung remodeling with basal ESC growth linked to nuclear IL-33 (nIL-33) control of cell growth and survival in concert with IL-33–independent AT2 cell growth. Subsequent production of Cxcl17 and secreted IL-33 (sIL-33) drives tissue macrophage (Mac) and ILC2 production of IL-13 for type 2 inflammation and mucinous differentiation. Together, these events result in local epithelial cell hyperplasia at bronchiolar and alveolar sites and, in turn, basal ESC migration and further growth and differentiation at bronchiolar-alveolar remodeling sites (generally designated as bronchiolization). These events are based on the present mouse model, recognizing that AT2 cells are not a significant source of IL-33 in humans, where intracellular and extracellular functions of IL-33 might be combined in basal cells.

remodeling (64). The markers for the relevant basal ESC subset identified in our study thus provide a roadmap for a precise, disease-modifying strategy relevant to the pressing and widespread consequences of severe respiratory viral infections.

Methods

Details on mouse line generation and treatment, RNA-Seq analysis, real-time qPCR assay, immunohistochemistry and immunocytochemistry, flow cytometry and FACS, epithelial cell culturing, scRNA-Seq analysis, scATAC-Seq analysis, and lung function testing are provided in the Supplemental Methods.

Data availability. The RNA-Seq and scRNA-Seq data were deposited in the NCBI's Gene Expression Omnibus (GEO) database (GEO GSE180392, RNA-Seq; GSE178517, scRNA-Seq; GSE178711, scATAC-Seq).

Study approval. All mouse husbandry and experimental procedures were approved by the Animal Studies Committees of the Washington University School of Medicine, in accordance with NIH guidelines.

Statistics. All data presented are expressed as the mean ± SEM. For these data, statistical differences between means for sample conditions were assessed using 1-way ANOVA with Bonferroni correction for multiple comparisons. For violin plot formats of single-cell gene expression data, statistical differences between the means for sample conditions were assessed using a Mann-Whitney U test with Bonferroni correction for multiple comparisons. For all data, the significance threshold was set at a P value of less than 0.05. The number of mice for each condition and the number of replicate experiments are indicated in the figure legends.

Author contributions

KW designed and performed mouse and cell experiments. KK, KY, MW, MEH, and SAM analyzed RNA-Seq data. YZ generated mouse strains. SPK performed mouse experiments. BJG assisted with cell culture experiments. EVA generated viruses. SPA performed histochemical analyses. JY performed cell culture experiments. KAG genotyped the mice. DEB processed tissue samples. JAB assisted with flow cytometry and mouse experiments. CMH analyzed RNA-Seq data. ECC reviewed the histology results. MJH directed the project and wrote the manuscript.

Address correspondence to: Michael J. Holtzman, Washington University School of Medicine, Campus Box 8052, 660 South Euclid Avenue, Saint Louis, Missouri 63110, USA. Phone: 314.362.8970; Email: mjholtzman@wustl.edu.

1. Gonzales KAU, Fuchs E. Skin and its regenerative powers: an alliance between stem cells and their niche. *Dev Cell*. 2017;43(4):387–401.
2. Andersson-Rolf A, et al. Stem cells in repair of gastrointestinal epithelia. *Physiology (Bethesda)*. 2017;32(4):278–289.
3. Swarr DT, Morrisey EE. Lung endoderm morpho-

genesis: gasping for form and function. *Annu Rev Cell Dev Biol*. 2015;31:553–573.
4. Zhang Y, et al. PARP9-DTX3L ubiquitin ligase targets host histone H2BJ and viral 3C protease to enhance interferon signaling and control viral infection. *Nat Immunol*. 2015;16(12):1215–1227.
5. Zhang Y, et al. Respiratory enterovirus (like para-

influenza virus) can cause chronic lung disease if protection by airway epithelial STAT1 is lost. *J Immunol*. 2019;202(8):2332–2347.
6. Tyner JW, et al. CCL5-CCR5 interaction provides antiapoptotic signals for macrophage survival during viral infection. *Nat Med*. 2005;11(11):1180–1187.

7. Pull SL, et al. Activated macrophages are an adaptive element of the colonic epithelial progenitor niche necessary for regenerative responses to injury. *Proc Natl Acad Sci U S A*. 2005;102(1):99–104.

8. Wu K, et al. Group 2 innate lymphoid cells must partner with the myeloid-macrophage lineage for long-term postviral lung disease. *J Immunol*. 2020;205(4):1084–1101.

9. Holtzman MJ, et al. The role of airway epithelial cells and innate immune cells in chronic respiratory disease. *Nat Rev Immunol*. 2014;14(10):686–698.

10. Keeler SP, et al. Influenza a virus infection causes chronic lung disease linked to sites of active viral RNA remnants. *J Immunol*. 2018;201(8):2354–2368.

11. Taylor MS, et al. A conserved distal lung regenerative pathway in acute lung injury. *Am J Pathol*. 2018;188(5):1149–1160.

12. Holtzman MJ. Asthma as a chronic disease of the innate and adaptive immune systems responding to viruses and allergens. *J Clin Invest*. 2012;122(8):2741–2748.

13. Chen J, et al. Long term outcomes in survivors of epidemic Influenza A (H7N9) virus infection. *Sci Rep*. 2017;7(1):17275.

14. Carfi A, et al. Persistent symptoms in patients after acute COVID-19. *JAMA*. 2020;324(6):603–605.

15. Giangreco A, et al. Terminal bronchioles harbor a unique airway stem cell population that localizes to the bronchoalveolar duct junction. *Am J Pathol*. 2002;161(1):173–182.

16. Kim CF, et al. Identification of bronchioalveolar stem cells in normal lung and lung cancer. *Cell*. 2005;121(6):823–835.

17. Rock JR, et al. Basal cells as stem cells of the mouse trachea and human airway epithelium. *Proc Natl Acad Sci U S A*. 2009;106(31):12771–12775.

18. McQualter JL, et al. Evidence of an epithelial stem/progenitor cell hierarchy in the adult mouse lung. *Proc Natl Acad Sci U S A*. 2010;107(4):1414–1419.

19. Chapman HA, et al. Integrin α6β4 identifies an adult distal lung epithelial population with regenerative potential in mice. *J Clin Invest*. 2011;121(7):2855–2862.

20. Tata PR, et al. Dedifferentiation of committed epithelial cells into stem cells in vivo. *Nature*. 2013;503(7475):218–223.

21. Lee, et al. Lung stem cell differentiation in mice directed by endothelial cells via a BMP4-NFATc1-thrombospondin-1 axis. *Cell*. 2014;156(3):440–455.

22. Ruiz EJ, et al. A paracrine network regulates the cross-talk between human lung stem cells and the stroma. *Nat Commun*. 2014;5:3175.

23. Barkauskas CE, et al. Type 2 alveolar cells are stem cells in adult lung. *J Clin Invest*. 2013;123(7):3025–3036.

24. Kumar PA, et al. Distal airway stem cells yield alveoli in vitro and during lung regeneration following H1N1 influenza infection. *Cell*. 2011;147(3):525–538.

25. Zuo W, et al. p63(+)Krt5(+) distal airway stem cells are essential for lung regeneration. *Nature*. 2015;517(7536):616–620.

26. Vaughan AE, et al. Lineage-negative progenitors mobilize to regenerate lung epithelium after major injury. *Nature*. 2015;517(7536):621–625.

27. Fang Y, et al. Distinct stem/progenitor cells proliferate to regenerate the trachea, intrapulmonary airways and alveoli in COVID-19 patients. *Cell Res*. 2020;30(8):705–707.

28. Byers DE, et al. Long-term IL-33-producing epithelial progenitor cells in chronic obstructive lung disease. *J Clin Invest*. 2013;123(9):3967–3982.

29. Wu K, et al. TREM-2 promotes macrophage survival and lung disease after respiratory viral infection. *J Exp Med*. 2015;212(5):681–697.

30. Byers DE, et al. Triggering receptor expressed on myeloid cells-2 expression tracks with M2-like macrophage activity and disease severity in COPD. *Chest*. 2018;153(1):77–86.

31. Gause WC, et al. Type 2 immunity and wound healing: evolutionary refinement of adaptive immunity by helminths. *Nat Rev Immunol*. 2013;13(8):607–614.

32. Graham BS, et al. Primary respiratory syncytial virus infection in mice. *J Med Virol*. 1988;26(2):153–162.

33. Walter MJ, et al. Viral induction of a chronic asthma phenotype and genetic segregation from the acute response. *J Clin Invest*. 2002;110(2):165–175.

34. Patel A. Genetic segregation of airway disease traits despite redundancy of calcium-activated chloride channel family members. *Physiol Genomics*. 2006;25(3):502–513.

35. Wang X, et al. TLR3-activated monocyte-derived dendritic cells trigger progression from acute viral infection to chronic disease in the lung. *J Immunol*. 2021;206(6):1297–1314.

36. Kim EY, et al. Persistent activation of an innate immune response translates respiratory viral infection into chronic lung disease. *Nat Med*. 2008;14(6):633–640.

37. Wolf FA, et al. Graph abstraction reconciles clustering with trajectory inference through a topology preserving map of single cells. *Genome Biol*. 2019;20(1):59.

38. La Manno G, et al. RNA velocity of single cells. *Nature*. 2018;560(7719):494–498.

39. Koga T, et al. Virus-inducible expression of a host chemokine gene relies on replication-linked mRNA stabilization. *Proc Natl Acad Sci U S A*. 1999;96(10):5680–5685.

40. Hutchins AP, et al. Distinct transcriptional regulatory modules underlie STAT3's cell type-independent and cell type-specific functions. *Nucleic Acids Res*. 2013;41(4):2155–2170.

41. Tyner JW, et al. Blocking airway mucous cell metaplasia by inhibiting EGFR antiapoptosis and IL-13 transdifferentiation signals. *J Clin Invest*. 2006;116(2):309–321.

42. Wheeler JC, et al. 17β-Estradiol protects the esophageal epithelium from IL-13-induced barrier dysfunction and remodeling. *J Allergy Clin Immunol*. 2019;143(6):2131–2146.

43. Dorward DA, et al. Tissue-specific immunopathology in fatal COVID-19. *Am J Respir Crit Care Med*. 2021;203(2):192–201.

44. Xi Y, et al. Local lung hypoxia determines epithelial fate decisions during alveolar regeneration. *Nat Cell Biol*. 2017;19(8):904–914.

45. Zacharias WJ, et al. Regeneration of the lung alveolus by an evolutionarily conserved epithelial progenitor. *Nature*. 2018;555(7695):251–255.

46. Chen H, et al. Airway epithelial progenitors are region specific and show differential responses to bleomycin-induced lung injury. *Stem Cells*. 2012;30(9):1948–1960.

47. Vieira Braga FA, et al. A cellular census of human lungs identifies novel cell states in health and in asthma. *Nat Med*. 2019;25(7):1153–1163.

48. Shiraishi M, et al. Alternatively activated macrophages determine repair of the infarcted adult murine heart. *J Clin Invest*. 2016;126(6):2151–2166.

49. Bosurgi L, et al. Macrophage function in tissue repair and remodeling requires IL-4 or IL-13 with apoptotic cells. *Science*. 2017;356(6342):1072–1076.

50. Lechner AJ, et al. Recruited monocytes and type 2 immunity promote lung regeneration following pneumonectomy. *Cell Stem Cell*. 2017;21(1):120–134.

51. Dagher R, et al. IL-33-ST2 axis regulates myeloid cell differentiation and activation enabling effective club cell regeneration. *Nat Commun*. 2020;11(1):4786.

52. Carriere V, et al. IL-33, the IL-1-like cytokine ligand for ST2 receptor, is a chromatin-associated nuclear factor in vivo. *Proc Natl Acad Sci U S A*. 2007;104(1):282–287.

53. Roussel L, et al. Molecular mimicry between IL-33 and KSHV for attachment to chromatin through the H2A-H2B acidic pocket. *EMBO Rep*. 2008;9(10):1006–1012.

54. Martin NT, Martin MU. Interleukin 33 is a guardian of barriers and a local alarmin. *Nat Immunol*. 2016;17(2):122–131.

55. Gautier V, et al. Extracellular IL-33 cytokine, but not endogenous nuclear IL-33, regulates protein expression in endothelial cells. *Sci Rep*. 2016;6:34255.

56. Pisabarro MT, et al. Cutting edge: novel human dendritic cell- and monocyte-attracting chemokine-like protein identified by fold recognition methods. *J Immunol*. 2006;176(4):2069–2073.

57. Burkhardt AM, et al. CXCL17 is a major chemotactic factor for lung macrophages. *J Immunol*. 2014;193(3):1468–1474.

58. Stier MT, et al. IL-33 promotes the egress of group 2 innate lymphoid cells from the bone marrow. *J Exp Med*. 2019;215(1):263–281.

59. Han M, et al. The innate cytokines IL-25, IL-33, and TSLP cooperate in the induction of type 2 innate lymphoid cell expansion and mucous metaplasia in rhinovirus-infected immature mice. *J Immunol*. 2017;199(4):1308–1318.

60. Page C, et al. Induction of alternatively activated macrophages enhances pathogenesis during severe acute respiratory syndrome coronavirus infection. *J Virol*. 2012;86(24):13334–13349.

61. Nie X, et al. Multi-organ proteomic landscape of COVID-19 autopsies. *Cell*. 2020;184(3):775–791.

62. Salahudeen AA, et al. Progenitor identification and SARS-CoV-2 infection in human distal lung organoids. *Nature*. 2020;588(7839):670–675.

63. Rao W, et al. Regenerative metaplastic clones in COPD lung drive inflammation and fibrosis. *Cell*. 2020;181(4):848–864.

64. Alevy Y, et al. IL-13-induced airway mucus production is attenuated by MAPK13 inhibition. *J Clin Invest*. 2012;122(12):4555–4568.